# Nanoparticles and microfluidics for future tuberculosis vaccines

Neustrup, M.A.

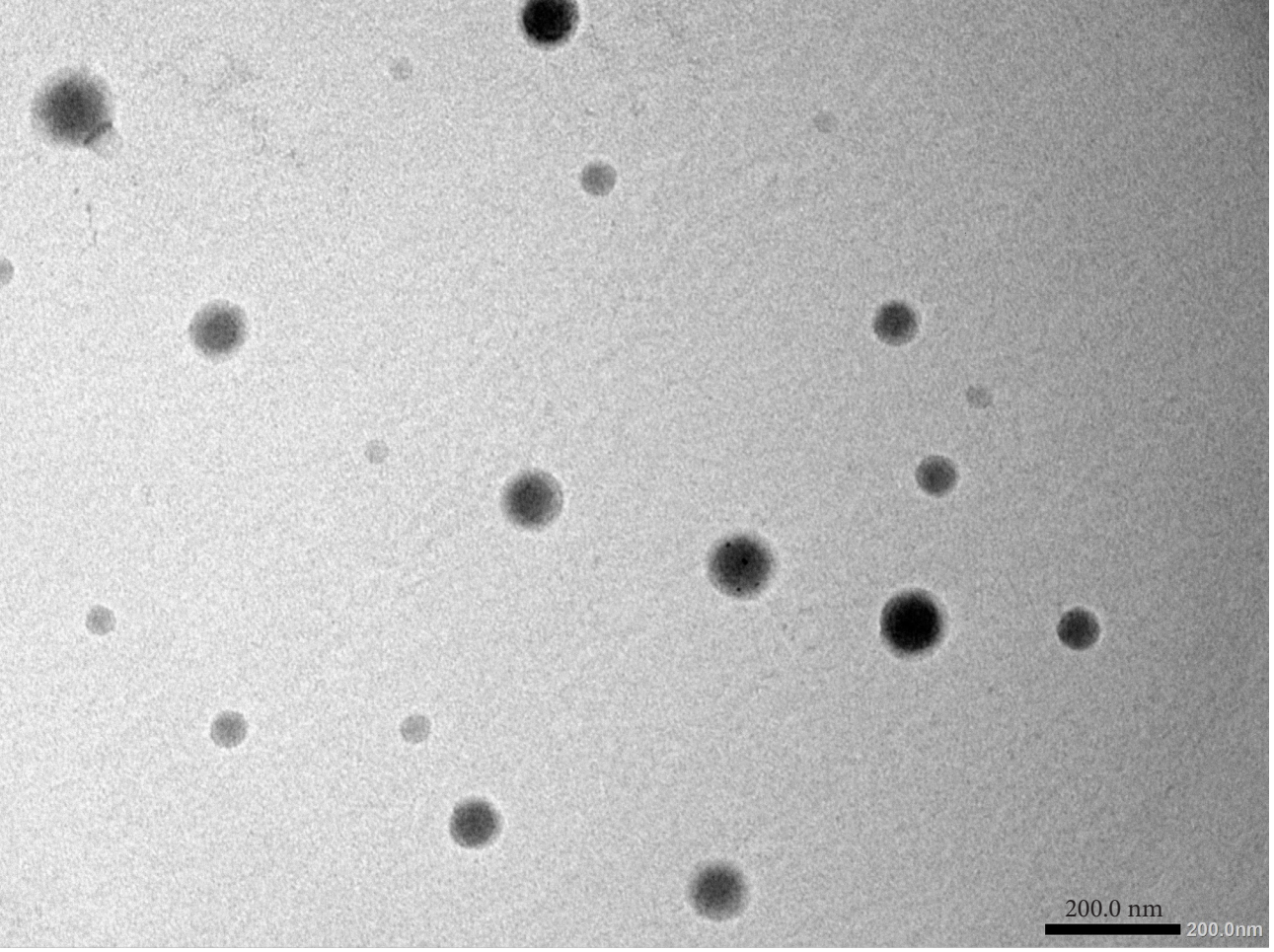


# CHAPTER 4

## EVALUATION OF PLGA, LIPID-PLGA HYBRID NANOPARTICLES, AND CATIONIC PH-SENSITIVE LIPOSOMES AS TUBERCULOSIS VACCINE DELIVERY SYSTEMS IN A *MYCOBACTERIUM TUBERCULOSIS* CHALLENGE MOUSE MODEL – A COMPARISON

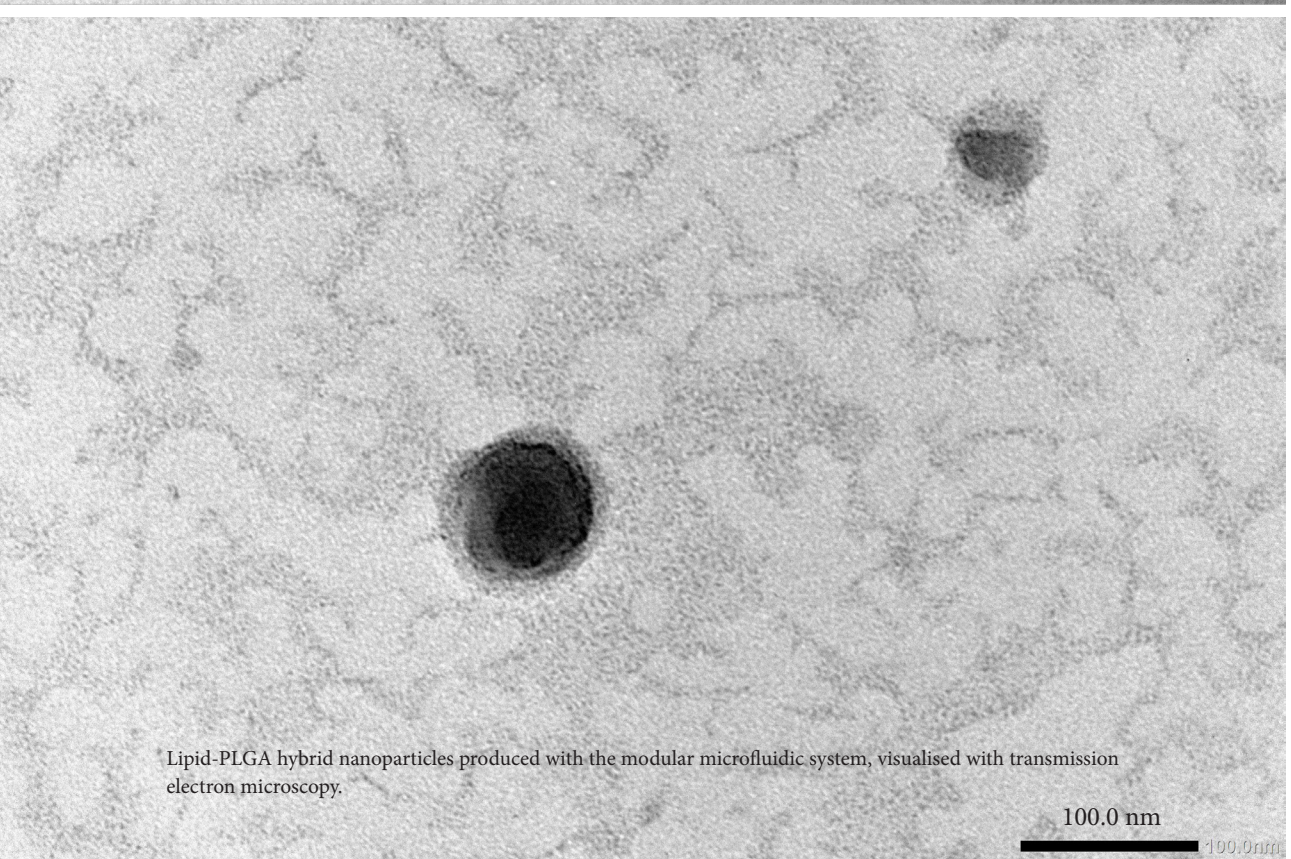


Lipid-PLGA hybrid nanoparticles produced with the modular microfluidic system, visualised with transmission electron microscopy.

Adapted from Int J Pharm. 2024;666:124842

M.M. Szachniewicz[1], M.A. Neustrup[2], S.J.F. van den Eeden[1], K.E. van Meijgaarden[1], K.L.M.C. Franken[1], S. van Veen[1], R.I. Koning[3], R.W.A.L. Limpens[3], A. Geluk[1], J.A. Bouwstra[2], T.H.M. Ottenhoff[1]

[1] Department of Infectious Diseases and LUCID, Leiden University Medical Center, Leiden, The Netherlands
[2] Division of BioTherapeutics, Leiden Academic Centre for Drug Research, Leiden University, Leiden, The Netherlands
[3] Electron Microscopy Facility, Leiden University Medical Center, Leiden, The Netherlands

# ABSTRACT

Tuberculosis (TB) continues to pose a global threat for millennia, currently affecting over 2 billion people and causing 10.6 million new cases and 1.3 million deaths annually. The only existing vaccine, *Mycobacterium Bovis* Bacillus Calmette-Guérin (BCG), provides highly variable and inadequate protection in adults and adolescents. This study explores newly developed subunit tuberculosis vaccines that use a multistage protein fusion antigen Ag85b-ESAT6-Rv2034 (AER). The protection efficacy, as well as *in vivo* induced immune responses, were compared for five vaccines: BCG; AER-CpG/MPLA mix; poly(D,L-lactic-co-glycolic acid) (PLGA); lipid-PLGA hybrid nanoparticles (NPs); and cationic pH-sensitive liposomes (the latter three delivering AER together with CpG and MPLA). All vaccines, except the AER-adjuvant mix, induced protection in *Mycobacterium tuberculosis* (Mtb)-challenged C57/Bl6 mice as indicated by a significant reduction in bacterial burden in lungs and spleens of the animals. Four AER-based vaccines significantly increased the number of circulating multifunctional $CD4^+$ and $CD8^+$ T-cells producing IL-2, IFN-γ, and TNFα, exhibiting a central memory phenotype. Furthermore, AER-based vaccines induced an increase in $CD69^+$ B-cell counts as well as high antigen-specific antibody titers. Unexpectedly, none of the observed immune responses were associated with the bacterial burden outcome, such that the mechanism responsible for the observed vaccine-induced protection of these vaccines remains unclear. These findings suggest the existence of non-classical protective mechanisms for Mtb infection, which could, once identified, provide interesting targets for novel vaccines.




# INTRODUCTION

The WHO estimates that approximately one quarter of the world's human population is latently infected with TB [1]. Dubbed the 'white plague', pulmonary TB is the primary transmissible form caused by *Mycobacterium tuberculosis* (Mtb) [2]. In 2022, 1.3 million died from TB, including 167,000 with HIV, making it a leading cause of death in this group of patients, and the second leading infectious disease killer after COVID-19, with the major cause of death due to antibiotic resistance [1]. TB is curable and preventable, but multidrug-resistant TB (MDR-TB) is an increasing public health threat [1]. The WHO aims to end the TB epidemic by 2030 as part of the United Nations' Sustainable Development Goals (SDGs) [3, 4]. As outlined by the End TB Strategy and the Western Pacific regional framework to end TB: 2021–2030 [5], the main tools to achieve this goal involve point-of-care approaches, early and easily accessible diagnostics, shorter and more effective treatment regiments, comprehensive treatment of all people with TB, including those with MDR-TB, management of co-morbidities, preventative treatment, and vaccination [3, 5].

Vaccination is indispensable for preventing infectious diseases like TB. Vaccines have enabled the eradication of smallpox and rinderpest and, more recently, have been essential in the fight against SARS-CoV-2 [6–8]. The only licensed TB vaccine *Mycobacterium Bovis* Bacillus Calmette-Guérin (BCG), unfortunately offers highly variable and often insufficient protection [9–11]. Therefore, there is an unmet demand for better vaccines against TB [10].

Subunit vaccines, produced with synthesized or purified antigens, DNA, or RNA, are safe and suitable for use in wide populations, including those with compromised immunity [12, 13]. This broad applicability is especially important for TB in countries with high HIV rates [5]. However, they often lack immunogenicity, making further improved delivery system development essential for subunit vaccines [14, 15]. Vaccine delivery systems use biocompatible nanoparticles (NPs) that prevent or limit antigen degradation and elimination, allow co-encapsulation of antigens with (molecular) adjuvants, and enhance uptake by antigen-presenting cells (APCs) [16–18]. The work presented in this paper investigates and compares the immunological and biological effects of poly(D,L-lactic-*co*-glycolic acid) (PLGA), lipid-PLGA hybrid NPs, and cationic pH-sensitive liposomes as particulate delivery systems for protein-based TB vaccines.

PLGA is one of the most extensively studied polymers for numerous biomedical applications. It is available in varied compositions and molecular weights. Its versatile characteristics make it suitable for tissue engineering and sustained-release drug and vaccine delivery systems. PLGA has excellent safety records, tunable degradation, release properties, and high versatility. This has led to its wide adoption in several biomedical applications and longstanding approval by the US Food and Drug Administration for human use including drug delivery, and various biomedical products ranging from sutures

to implants [17, 19–24]. It biodegrades through hydrolysis into non-toxic metabolic by-products lactic and glycolic acid [23]. Previous studies have demonstrated the efficacy of antigen- and adjuvant-loaded PLGA nanoparticles in enhancing cell-mediated immune response in mice [25–32].

Cationic liposomes are potent delivery systems that serve as particulate adjuvants [12, 16, 33–35]. Several liposome-based vaccines have been approved for clinical use [36–38]. Specifically, cationic liposomes can enhance immune responses, inducing the maturation of DCs and triggering T-cell responses, making them a versatile vaccination platform [39–41].

pH-sensitive liposomes are a subclass of (cationic) liposomes that respond to pH changes by altering their molecular bilayer organization upon a decrease in pH. When exposed to an acidic environment, bilayers destabilize, which results in a fusion of the liposome with the endosomal membrane, thus releasing their cargo. This allows them to deliver antigens and adjuvants into a cell's cytosol, avoiding endosomal degradation [42–46]. This unique ability to escape rapid degradation has potential vaccination benefits [47]. Unlike non-pH-sensitive liposomes that degrade inside the endosome [48, 49] pH-sensitive liposomes can protect antigens and facilitate cross-priming [49, 50], which could significantly impact the type of immune responses induced by a vaccine [51].

Lipid-PLGA hybrid NPs are complex nanostructures that have been successfully used in drug and vaccine delivery in preclinical research [52–56]. These hybrid NPs comprise a biodegradable PLGA core enveloped in a lipid shell that encapsulates drugs or antigens. They combine the properties of both PLGA NPs and liposomes. PLGA provides a rigid and solid core that allows sustained controlled release of antigens and adjuvants whereas the (cationic) lipid shell overcomes the lack of the immunogenicity of PLGA, facilitates uptake by APCs, reduces the degradation rate of the PLGA core by limiting water diffusion into the particle, thus ensuring controlled release kinetics [52, 54, 57, 58]. In vaccine applications, cationic lipid-PLGA hybrid NPs have demonstrated enhanced immunogenicity and induced humoral and cellular immune responses [58–64].

In this study, the immunogenicity and effectiveness of tuberculosis vaccines prepared with NP-based delivery systems were compared to the antigen-adjuvant mixture in mice. The fusion protein antigen Ag85B-ESAT6-Rv2034 (AER) combined with adjuvants monophosphoryl lipid A (MPLA), cytosine-phosphate-guanine motifs oligodeoxynucleotides (CpG ODN) were used in the formulation. AER consists of Ag85B, an immunodominant antigen rich in epitopes offering enhanced protection when combined with other antigens [65]; ESAT6 which is a potent immunomodulatory antigen that is not expressed by BCG [21, 66]; both used in vaccines currently in clinical trials: H1:IC31 [67], and H56:IC31 [68]; and Rv2034 which is a potent *in vivo* expressed Mtb antigen [69]. AER mixed with CAF09 adjuvant induced protection in HLA-DR3 transgenic mice and in guinea pigs [70]. CpG is a Toll-like receptor (TLR) 9 ligand that induces robust Th1 responses, and MPLA, a TLR4 agonist, induces Th1 and Th17 responses [71–73]. A combination of both has been successfully used in several phase II and III clinical trials, and it was demonstrated safe and effective in the induction of robust T-cell and antibody responses [74–78]. The novel tuberculosis subunit vaccines developed in this research were tested *in vitro* on primary human APCs for immunogenicity and *in vivo* on C57Bl/6 mice with intranasal H37Rv Mtb infection to quantify protection, specifically CFU reduction in lungs and spleens. Immune responses in vaccinated, non-Mtb challenged mice were analyzed using a 27-marker spectral flow cytometry for $CD4^+$, $CD8^+$ T-cells, and B-cell responses. Additionally, serum antigen-specific antibody titers were measured.

# MATERIALS AND METHODS

## Materials

1,2-dioleoyl-sn-glycero-3-phosphocholine (DOPC), 1,2-dioleoyl-sn-glycero-3-ethyl-phosphocholinechloride salt (EPC), 1,2-dioleoyl-sn-glycero-3-phosphoethanolamine (DOPE), N-(4-carboxybenzyl)-N,N-dimethyl-2,3-bis(oleoyloxy)propan-1-aminium (DOBAQ), and monophosphoryl lipid A, PHAD (MPLA) were purchased from Avanti Polar Lipids, Inc. in the USA. Fig. S1 illustrates the chemical structures of these lipids. Class B CpG oligonucleotide ODN1826 was acquired from InvivoGen (the Netherlands). PLGA (acid terminated, lactide:glycolide 50:50, Mw 24,000-38,000) was purchased from Merck Chemicals B.V. (the Netherlands). Interconnect tees for use with 360 µm outer diameter capillaries, one-piece fittings (for 360 µm capillaries and for 1/16" tubings), two-piece adapters (360-µm-to-1.6-mm and 1.6-mm-to-360-µm), and Luer-lock adapters (for use with 360 µm capillaries and 1/16" tubings), were obtained from Mengel Engineering (Denmark). Polyether ether ketone capillary tubing (inner diameter of 0.02" and outer diameter of 1/16"), was bought from Fisher Emergo B.V. (the Netherlands). A Teflon tube (1/16") was sourced from Waters Chromatography B.V. (the Netherlands). TSP Standard polyimide-coated fused silica tubings, (75 µm and 250 µm inner diameters, and 360 µm outer diameter) were obtained from BGB Analytik Benelux B.V. (the Netherlands). Polytetrafluoroethylene Luer-lock Hamilton gastight (1710TLL 100 µL, 1001TLL 1 ml, and 1010TLL 10 ml) syringes were purchased from Merck (Germany). Recombinant fusion protein AER was produced as described by Franken et al. [79]. Briefly, genes from Mtb (lab strain H37Rv) were amplified using PCR with genomic DNA. The amplified genes were cloned into bacteria using an N-terminal hexa-histidine (His) tag utilizing Gateway technology (Invitrogen, USA), and their successful insertion was confirmed through sequencing. The antigen AER was then expressed in *Escherichia coli* strain BL21 (DE3) and purified. Its quality was assessed through gel electrophoresis followed by Coomassie brilliant blue staining and with an anti-His antibody (Invitrogen, USA) Western blotting, which evaluated the size and purity of the protein. The ToxinSensor

Chromogenic Limulus Amebocyte Lysate (LAL) Endotoxin Assay Kit (GenScript, USA) was employed to determine the endotoxin contamination level in the protein, revealing levels below 50 endotoxin units per 1 mg of protein.

### Liposome production

Liposomes were made using the thin-film hydration method, as described previously [80]. Lipids were dissolved in chloroform and diluted from 25 mg/ml stocks to 10 mg per batch. The composition used was DOPC:DOPE:DOBAQ:EPC in a molar ratio 3:5:2:4. The lipid solution was placed in a flask and chloroform was removed using a Buchi rotavapor R210 (Switzerland). The lipid film was then rehydrated with 1 ml of 200 µg/ml AER in 10 mM phosphate buffer (PB) at pH 7.4 to create AER-containing liposomes. These were downsized with Branson sonifier 250 (US) using an eight-cycle sonication program comprising 30 s of sonication at 10% amplitude, followed by a 60-s break, and centrifuged (at 500 g for 3 min) to remove metal particles. The liposomal suspensions (5 mg/ml lipids) were transferred to new tubes and stored at 4 °C overnight. The final product contained 40 µg/ml AER and 2 mg/ml lipids after dilution with  10 mM PB.

### PLGA NP preparation

The PLGA NPs were produced using a modular microfluidic system. A three-component system was used for PLGA NPs. Briefly, the contents of two syringes, Syringe 1 and 2, met each other in a T-flow, subsequently, the combined fluid met the contents of a third syringe, Syringe 3, in a co-flow, where the combined fluid constitutes the inner flow and the content of Syringe 3 constitutes the outer flow. The three syringes contained: 1) 3.33 mg/ml AER solution and 1 mg/ml CpG in water for injection, 2) 5 mg/ml PLGA and 12.5 µg/ml MPLA in acetonitrile, and 3) water for injection. The flow rates for the fluids in Syringe 1, 2, and 3 were set to 37.5, 1250, and 4955 µl/min, respectively, obtaining a total flow rate of 6242.5 µl/min, and final concentrations of 20 µg/ml AER, 6 µg/ml CpG, 2 mg/ml PLGA, and 2.5 µg/ml MPLA. The suspensions were set under a stream of nitrogen to evaporate the acetonitrile and concentrate the formulations. Before the characterization of particles and further use *in vitro* and *in vivo*, a concentrated solution of PB was added to obtain a concentration of 10 mM PB in the final product (40 µg/ml AER, 12 µg/ml CpG, 2 mg/ml PLGA, and 5 µg/ml MPLA).

### Lipid-PLGA hybrid NP preparation

The lipid-PLGA NPs were produced using the same method as PLGA NPs with modifications. A four-component system was used in this case. As described above, AER solution with CpG was combined with PLGA (without MPLA) solution in an interconnected tee. The combined flow (1287.5 µl/min) was then directed into another tee, where it was combined with water for injection (at 3712 µl/min), and 5 mg/ml lipid solution of DOPC:DOPE:DOBAQ:EPC (3:5:2:4) containing 12.5 µg/ml MPLA in ethanol at a flow rate of 1250 µl/min. The total flow rate was 6249.5 µl/min. The produced suspension was then evaporated and twice up-concentrated under nitrogen flow. The final product contained 40 µg/ml AER, 12 µg/ml CpG, 2 mg/ml PLGA, 2 mg/ml lipids, 5 µg/ml MPLA, and 10 mM PB.

### Determination of size and zeta-potential

The hydrodynamic diameter (Z-average size) and polydispersity index (PDI) of the liposomal formulations were determined with dynamic light scattering (DLS), and zeta potential was measured using laser Doppler electrophoresis as described previously [80]. Liposomes were diluted to 0.25 mg/ml lipid in 10 mM PB at pH 7.4 and added to 1.5 ml VWR Two-Sided Disposable PS Cuvettes (VWR, the Netherlands). Measurements, conducted in triplicates with at least ten runs at 20 °C, were performed using a Nano ZS Zetasizer with 633 nm laser and 173° optics (Malvern Instruments, UK). The data were analyzed with Zetasizer Software v7.13 (Malvern Instruments).

### Differentiation of human monocyte-derived dendritic cells (MDDCs) and macrophages (MDMFs)

After written informed consent, PBMCs were obtained from healthy donors' buffy coats (Sanquin Blood Bank, Netherlands) as described previously [80]. Using the Ficoll-based density gradient centrifugation method, PBMCs were separated, and $CD14^+$ cells were isolated via the magnetic cell isolation method (MACS) with an autoMACS Pro Separator (Miltenyi Biotec BV, the Netherlands). These cells were then differentiated into DCs, and type 1 and 2 (M1 and M2, respectively) macrophages over six days using cytokines. MDDCs were generated with 10 ng/ml recombinant human granulocyte-macrophage colony-stimulating factor (GM-CSF; Miltenyi Biotec BV, the Netherlands) and 10 ng/ml recombinant human interleukin 4 (IL-4; Peprotech, USA). For M1 macrophages we used 5 ng/ml GM-CSF, and for M2 macrophages we used 50 ng/ml macrophage colony-stimulating factor (M-CSF; Miltenyi Biotec BV, the Netherlands) [81]. Cells were cultured at 37 °C/5% $CO_2$ in Roswell Park Memorial Institute (RPMI) 1640 medium, supplemented with 10% fetal bovine serum (FBS), penicillin (100 units/ml), streptomycin (100 µg/ml), and 2 mM GlutaMAX (Gibco, Belgium). MDDCs were harvested through pipetting, while for macrophages, we used trypsinization (Gibco, Belgium).

### Uptake study

To assess the uptake of liposome, MDDCs, M1, and M2 MDMFs were cultured in 96-well plates with round bottoms (CELLSTAR, Greiner Bio-One GmbH, Germany), each well containing 30,000 cells. These cells were then treated with 1% (v/v) empty fluorescent liposomes containing 0.1% mol% of 1,2-dioleoyl-*sn*-glycero-3-phosphoethanolamine-N-(Cyanine 5) (18:2 PE-Cy5) sourced from Avanti Polar Lipids, Inc., USA, for 1 h. Following exposure, the cells were washed three times with FACS buffer to eliminate any free liposomes. Flow cytometry data collection was collected using a BD FACSLyric Flow Cytometer (BD Biosciences, Belgium), and the analysis of this data was conducted using the FlowJo software, version 10.6 (FlowJo LLC, BD, USA) [80].

### Activation study

The adjuvant properties of formulations loaded with AER were investigated using MDDCs as described previously [82]. To 30,000 cells/well in MDDCs seeded in 96-well plates with round bottoms (CELLSTAR, Greiner Bio-One GmbH, Germany), at a density of 30,000 cells per well, with lipid concentrations ranging from 25 to 250 µg/ml in 200 µl of medium. The cells were incubated for 1 h at 37 °C/5% $CO_2$. Subsequent to this incubation, cells were rinsed with a complete RPMI medium and then cultured overnight. The following day, cells were centrifuged, the supernatants collected and stored at -20 °C for later use. For flow cytometry, cells were washed with FACS buffer (PBS with 0.1% bovine serum albumin; Merck, Germany) and blocked for 5 min with 5% human serum (Sanquin Blood Bank, the Netherlands) in PBS to prevent non-specific Fc-receptor binding. After blocking, cells were stained for 30 min with monoclonal antibodies targeting various cell surface markers: CCR7-BB515 (clone 3D12, catalog 565870), CD83-PE (clone HB15e, catalog 556855), CD40-APC (clone 5C3, 555591), CD80-APC-R700 (clone L307.4, catalog 565157), HLA-DR-V500 (clone G46-6, 561225) from BD Biosciences, Belgium, and CD86-BV421 (clone IT2.2, 305426) from BioLegend, the Netherlands, all at a dilution of 1:200 in FACS buffer. Post-staining, cells were again washed three times and resuspended in FACS buffer. Flow cytometry data was acquired using a BD FACSLyric Flow Cytometer and analyzed with FlowJo software.

### Luminex assay

According to the manufacturer's protocols, supernatants were tested in two Bio-Plex panels (Bio-Rad, Veenendaal, the Netherlands). In total, 16 analytes were measured. The chemokine panel consisted of CXCL9, CXCL11, CCL8, and CCL22. The cytokine panel included CCL11 (Eotaxin), GM-CSF, IFN-α2, IL-1β, IL-1rα, IL-6, CXCL10, CCL2(MCP-1), CCL3, CCL4, RANTES and TNF-α. Samples were acquired on a Bio-Plex 200 system and analyzed with Bio-Plex manager software version 6.1.

### Mice

All mouse experiments were individually designed, reviewed, ethically approved, and registered by the institutional Animal Welfare Body of the Leiden University Medical Center (LUMC). The study was conducted under project license AVD116002017856, issued by the Netherlands's Central Authority for Scientific Procedures on Animals (CCD). The experiments adhered to the Dutch Act on Animal Experimentation and EU Directive 2010/63/EU for animal experiments.



The Jackson Laboratory (USA) provided C57Bl/6 mice (stock number SC1300004), which were housed in the LUMC animal facility. Female mice, aged 6–8 weeks and matched for age (17–18 g weight), were utilized for each experiment. Mice were housed in a specific pathogen-free, temperature-controlled environment (20 °C ± 1 °C; humidity 55% ± 15%,) including a controlled day-night cycle (12 h per day; 60-300 lux), in individually ventilated cages containing bedding and nesting materials and as enrichment a tunnel and gnawing wood with no more than six mice per cage. Food and drinking water *ad libitum*. Mice were acclimatized for one week following transport before the experiments began.

Two independent experiments were performed. The experimental groups, summarized in Table 1, included naïve (unimmunized) mice as a negative control and a BCG immunized group as a control group using the licensed TB vaccine. Each mouse was considered an experimental unit, and mice in the same experimental group were housed together in one cage. Each group consisted of six mice, and a total of 36 mice were used per experiment. The results from the two experiments were combined for statistical analysis, increasing the number of mice to 12 per group and 72 in total.

### Immunizations

C57Bl/6 mice were randomly allocated to six groups (6 mice per group). The naïve group served as the unimmunized control. Mice in the remaining groups were vaccinated with either BCG or AER combined with CpG (ODN1826) and MPLA (PHAD) or with AER together with CpG and MPLA delivered in PLGA NPs, cationic pH-sensitive liposomes or pH-sensitive lipid PLGA hybrid NPs. For immunizations that involved nanoparticle-based delivery systems, mice were given 3 subcutaneous (s.c.) injections in the right flank every 2 weeks with appropriate formulations (Table 1). Four weeks post-final immunization, mice were either sacrificed or infected with live Mtb. When AER was mixed with adjuvants, mice received 3 injections every 2 weeks with a solution of 25 µg AER, 50 µg CpG, and 1 µg MPLA in 200 µl PBS. For BCG vaccination, mice were given a single s.c. injection with $10^6$ CFU live BCG (Danish strain 1331) 12 weeks prior to sacrifice or Mtb infection. BCG bacterial counts were determined by placing the suspension on 7H10 agar plates (Difco, BD, Franklin Lakes, NJ USA) supplemented with BBL Middlebrook OADC enrichment (BD, Franklin Lakes, NJ USA) and counting colonies after a 3-week incubation at 37 °C. Doses, frequency, and routes of administration were selected based on previous research [70, 80, 83].

**Table 1**. Summary of vaccination groups and doses of vaccine constituents administrated to a mouse in a single immunization. Each group consists of 6 mice per experiment. All adjuvanted systems also contained CpG and MPLA. NA: not applicable.

| Group | Description | AER (µg) | Lipid (µg) | PLGA (µg) | CpG (µg) | MPLA (µg) |
|---|---|---|---|---|---|---|
| Naïve | Unimmunized | NA | NA | NA | NA | NA |
| BCG | Approved vaccine | NA | NA | NA | NA | NA |
| Ag | Antigen-adjuvant mix | 25 | NA | NA | 50 | 1 |
| PLGA | PLGA NPs | 8 | NA | 400 | 2.5 | 1 |
| Hybrid | Lipid-PLGA hybrid NPs | 8 | 400 | 400 | 2.5 | 1 |
| pH | pH-sensitive liposome | 8 | 400 | NA | 2.5 | 1 |

### Intranasal infection with H37Rv Mtb

Unimmunized and immunized mice were infected with live Mtb H37Rv either 4 weeks post-AER vaccination or 12 weeks after BCG vaccination. Mice were sedated using isoflurane (Pharmachemie BV, The Netherlands) and received an intranasal dose of $10^5$ CFU Mtb sourced from glycerol stocks kept at at -80 °C [84]. The bacterial count was measured using 7H10 agar plates. The bacterial colonies were counted after incubation for 3 weeks at 37 °C. Six weeks following the Mtb infection, the mice were humanely euthanized using $CO_2$. Their spleens and lungs were aseptically extracted. These tissues were then processed using 70 µM mesh strainers (Corning, USA) in a sterile PBS solution. The counts of bacteria were evaluated by serial dilutions on 7H11 agar plates (procured from BD Bioscience, USA), which were supplemented with OADC and PANTA (sourced from BD, Franklin Lakes, NJ USA).

### Splenocyte cultures

Splenocytes from immunized uninfected mice were resuspended at $3 \times 10^6$ cells/ml in Iscove's Modified Dulbecco's Medium (IMDM; Lonza, Switzerland) with 2 mM GlutaMAX™, 100 U/100 µg/ml penicillin-streptomycin (both purchased from Gibco, Paisley, UK), and 8% heat-inactivated fetal bovine serum (FBS; Greiner, Frickenhausen, Deutschland), and stimulated *in vitro* with 5 µg/ml of AER or its single components at 37 °C and 5% $CO_2$. After 6 days, the splenocytes were restimulated with the same protein for 5 h, and 2.5 µg/ml Brefeldin A (Sigma, Merck, Darmstadt, Germany) was added overnight. They were then harvested and stained for intracellular cytokines and surface markers the next day, as described previously [83].

### Antibody enzyme-linked immunosorbent assay (ELISA)

Blood was drawn from immunized, uninfected mice via heart puncture and cooled on ice. It was then centrifuged at 15,000 rpm for 10 min to obtain sera. ELISA was used to determine antibodies against proteins in sera, as described previously [83]. Plates were coated overnight with AER (5 µg/ml) or PBS/0.4% BSA (Sigma, Merck, Darmstadt, Germany) at 4 °C and blocked for 2 h with PBS/1% BSA/1% Tween-20. Serum dilutions (100 µl/well) were kept at 37 °C for 2 h, followed by a wash (PBS, 0.05% Tween-20) and incubation with horse radish peroxide (HRP)-labeled rabbit-anti-mouse antibodies: total IgG, IgG1, IgG2a, IgG2b, IgG2c, IgG3, and IgM (Dako, Denmark). After a 2-h incubation at 37 °C, plates were washed and treated with 100 µl/well tetramethylbenzidine substrate (TMB; Sigma) for 15 min. Then $H_2SO_4$ was added, and OD450 was measured using a Spectramax i3x spectrometer Molecular Devices, CA, USA).

### Antibody staining and flow cytometry

Surface and intracellular staining procedures were described elsewhere [83]. In short, splenocytes were transferred to 96-well plates and washed with PBS. They were stained with Zombie UV Fixable Viability Kit (BioLegend, the Netherlands), diluted 1:250 in PBS, and incubated with 100 µl of dye per well for 30 min. The cells were washed twice with FACS buffer (PBS with 0.1% BSA), blocked with 20 µl of 5% normal mouse serum (Thermo Fisher Scientific Inc., Bleiswijk, the Netherlands) in FACS buffer, then washed and stained with CCR7 for 30 min at 37 °C. The full list of antibodies used is summarized in Table S1. Lastly, the cells were washed twice and stained with a 50 µl/well antibody mix containing 10 µl/well of BD Horizon Brilliant Stain Buffer Plus (BD Biosciences, Belgium). Cells were incubated at 4 °C for 30 min, washed twice with FACS buffer, and then fixated and permeabilized with eBioscience Foxp3/Transcription Factor Staining Buffer Set (Invitrogen, Thermo Fisher Scientific, Belgium) at 4 °C for 60 min.

Following a wash, intracellular staining was performed using a diluted antibody mix in permeabilization buffer. Cells were incubated with 50 µl/well antibody mix for 45 min, washed twice with FACS buffer, and resuspended in 100 µl/well FACS buffer. They were then stored at 4 °C until measured with a Cytek Aurora spectral flow cytometer (Cytek Biosciences, Fremont, CA, USA) at the Flow Cytometry Core Facility of Leiden University Medical Center in the Netherlands.

### Flow cytometry data analysis

Data were analyzed with FlowJo v10.8.0 and OMIQ (www.omiq.ai) software, as described previously [83]. The analysis strategy is shown in Fig. S2. In brief, data were first manually gated in FlowJo to remove debris, doublets, and acquisition-disturbed cells. Cells were then gated on CD3 vs CD19, and T-cells ($CD3^+CD19^-$) and B-cells ($CD3^-CD19^+$) were separately exported (min. 20,000 events each) to OMIQ. The imported data were further cleaned with FlowAI in OMIQ, and single marker gates were created. Using Boolean gating, gate combinations were made. Counts for all Boolean gates were exported, and statistical analysis was conducted. Uniform manifold approximation and projection (UMAP) was performed on digitally concatenated cells from all mice in each group.

### Cryo-electron microscopy

Cryo-electron microscopy was performed as described previously [85]. Quantifoil 2/2 electron microscopy grids were glow discharged in 0.2 mbar air, at 25 mA, and for 30 s using an Easyglow (Pelco). A 3 µl droplet of the sample was added to the glow discharged grids, and blotted away using filter paper (Whatman no.4) for 3 s at 85–95% humidity and room temperature, using an EM GP (Leica). The grid was subsequently plunged into liquid ethane/propane (2:1) at -196 °C. Grids were transferred into a Talos Arctica (Thermo Fisher Scientific) and images were acquired using EPU (Thermo Fisher Scientific) in multi-grid mode, at 0.55 nm/pixel, 15000x nominal magnification. Images were recorded on a K3 direct electron detector (Gatan) in counting mode and ZLP imaging in movie mode, a defocus of -5 µm, and an electron dose of ~ 4 e/A2/s with 8 s exposure time (corresponding to a total dose of 35 e/A2). Using this magnification/pixel size and electron dose, the full 2-µm hole is visible in one image, and the vesicle bilayer (at 4 nm) can be discerned. Movies (80 frames in total) were aligned using MotionCor2 and converted to tiff using EMAN2.

### Statistical analysis

Mann-Whitney statistical test with Benjamini Hochberg FDR correction was carried out using R [86] and RStudio [87], to identify differentially abundant populations of cells. Statistical analyses to compare vaccination groups were performed in GraphPad Prism, version 8.01 (GraphPad Software, Prism, USA), using the Kruskal-Wallis test and an uncorrected Dunn's posthoc test for non-parametric comparisons of three or more groups to the control group, where cutoff of $P < 0.05$ was selected as statistically significant (*$P < 0.05$, **$P < 0.01$, ***$P < 0.001$, ****$P < 0.0001$). Bar values represent the median and error bars the interquartile range (IQR) unless indicated otherwise.

## RESULTS

### In vitro testing of vaccine formulations

Formulations were prepared using three types of nanoparticle-based vaccine delivery systems: PLGA NPs, lipid-PLGA hybrid NPs, and cationic pH-sensitive liposomes. Both hybrid NPs and liposomes shared the same lipid composition DOPC:DOPE:DOBAQ:EPC (3:5:2:4). We performed the initial immunogenicity tests in primary human MDDCs, including the performance of PLGA NPs.

First, we examined the uptake of PLGA NPs (Fig. S2). The uptake was assessed using primary human MDDCs (IL-4 and GM-CSF-induced), as well as pro-inflammatory M1 (GM-CSF-induced) and anti-inflammatory (M-CSF-induced) MDMFs. The uptake of empty PLGA NPs in MDDCs was much lower compared to the uptake observed in type 1 and 2 MDMFs (Fig. S2a). Because the PLGA NPs were not positively charged and no targeting moieties were used, it was expected that the uptake in DCs would be low.



Subsequently, the uptake of empty PLGA and empty cationic lipid-PLGA hybrid NPs was compared in MDDCs only (the primary APCs of our interest) (Fig. S2b). A significantly higher uptake was measured for the lipid-PLGA hybrid NPs compared to the PLGA NPs. Similarly to our previous work, pH-sensitive liposomes were efficiently taken up by all three types of APCs (manuscript submitted). These results thus show that professional APCs relatively poorly take up PLGA NPs without any adjuvants.

Subsequently, we examined the activation of primary human MDDCs in terms of the expression of cell-surface activation markers and cytokine production (Fig. S3 and S4). Unadjuvanted PLGA, lipid-PLGA NPs, and pH-sensitive liposomes were tested, as well as their counterparts formulated with CpG and MPLA adjuvants. Unadjuvanted PLGA NPs, as expected, were weakly immunogenic, failed to increase activation marker expression, and induced weak or non-detectable cytokine production. Unadjuvanted lipid-PLGA hybrid NPs were more efficient in activating MDDCs in terms of cell surface markers and cytokine production than the PLGA NPs. Cationic pH-sensitive liposomes induced CD40, CD83, and CCR7 expression but did not induce cytokine production. However, PLGA and lipid-PLGA NPs adjuvanted with CpG and MPLA induced both cell-surface markers expression and cytokine production. These results indicated that inert PLGA NPs, when formulated with potent adjuvants, can induce robust immune responses in vitro and, therefore, are promising delivery systems.

### Physicochemical characterization of vaccine formulations and mouse study design

PLGA, lipid-PLGA hybrid NPs, and cationic pH-sensitive liposomes formulated with AER antigen, CpG, and MPLA adjuvants were prepared and characterized (Table 2). PLGA NPs had the smallest size about 85 nm, and very low Zeta-potential of about -50 mV. Lipid-PLGA hybrid NPs and liposomes had higher sizes of about 140 nm and 170 nm, respectively, as well as Zeta-potential between 20 ÷ 25 mV. Cryo-electron microscopy (Fig. S5A) revealed spherical PLGA NPs in the size range between 50 and 100 nm with unsharp edges. Cryo-electron images of lipid-PLGA hybrid NPs (Fig. S5B) revealed spherical NPs with clear lipid bilayer-resembling features. Subsequently, formulations were administrated subcutaneously to mice three times two weeks apart. Naïve (unimmunized) mice and BCG and AER mixed with CpG and MPLA were used as control groups. The immunization groups are summarized in Table 1. In the AER-adjuvant mix group, higher doses of antigen (25 µg compared to 8 µg) and CpG (50 µg compared to 2.5 µg) were used.

**Table 2**. Physicochemical properties of liposomes used for immunization of mice. Results represent a mean of n = 6 batches (3 batches used in 2 experiments, each batch value is a mean of a triplicate) and standard deviation.

| Formulation | Z-average size (nm) | PDI (-) | Zeta-potential (mV) |
|---|---|---|---|
| AER/PLGA | 83.9 ± 17.8 | 0.25 ± 0.10 | -49.6 ± 11.2 |
| AER/DOPC:DOPE:DOBAQ:EPC/PLGA | 139.7 ± 8.0 | 0.19 ± 0.03 | 25.1 ± 1.8 |
| AER/DOPC:DOPE:DOBAQ:EPC | 166.9 ± 41.6 | 0.34 ± 0.09 | 21.5 ± 3.2 |

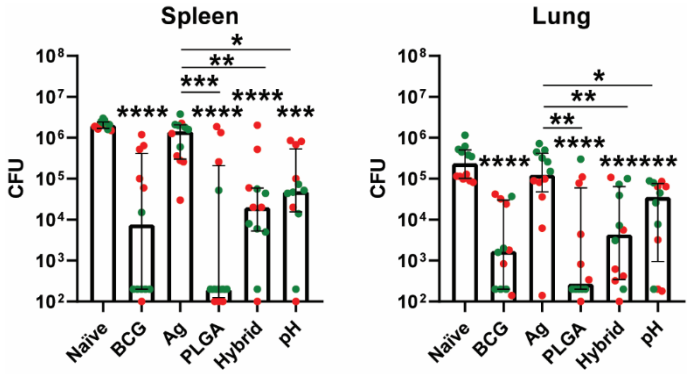


**Figure 1**. Bacterial burden in spleens (a) and lungs (b) of challenged mice represented by colony forming units (CFU) of Mtb. Each point represents CFU obtained from a single mouse. Colors indicate mice used in the same experiment. Groups: naïve – unimmunized mice; BCG – live BCG; Ag –antigen (25 μg Ag85B-ESAT6-Rv2034, AER) adjuvant mix (50 μg CpG, 1 μg MPLA), NP-free; PLGA – antigen (8 μg AER) and adjuvants (2.5 μg CpG, 1 μg MPLA) delivered in PLGA (400 μg) NPs; Hybrid – antigen (8 μg AER) and adjuvants (2.5 μg CpG, 1 μg MPLA) delivered in lipid (400 μg DOPC:DOPE:DOBAQ:EPC, 3:5:2:4)-PLGA (400 μg) NPs; pH – (8 μg AER) antigen and adjuvants (2.5 μg CpG, 1 μg MPLA) delivered in cationic pH-sensitive liposomes (400 μg DOPC:DOPE:DOBAQ:EPC, 3:5:2:4). n = 12. Bars represent median ± IQR. *$p < 0.05$, **$p < 0.01$, ***$p < 0.001$, ****$p < 0.0001$ (Kruskal-Wallis with an uncorrected Dunn's posthoc test).

### Nanoparticle-based subunit vaccines induce protection against Mtb in mice

The bacterial burden in lungs and spleens of infected mice was examined six weeks after the infection, which corresponds to ten weeks after the last immunizations (Fig. 1). Bacterial counts from mice vaccinated with PLGA, lipid-PLGA, and pH-sensitive liposomal formulations as well as BCG were all significantly reduced compared to unimmunized mice and mice vaccinated with AER-adjuvant mix both in lungs and spleens, mounting to 2–3 log differences. Mice vaccinated with PLGA NPs had lower median CFUs, both in spleens and lungs, compared to BCG and the other two NP-based vaccines; however, the difference was not statistically significant between these groups. Noteworthy, NP-based vaccines used much lower doses of the antigen (8 μg vs 25 μg) and CpG (2.5 μg vs 50 μg) compared to the antigen-adjuvant mix.



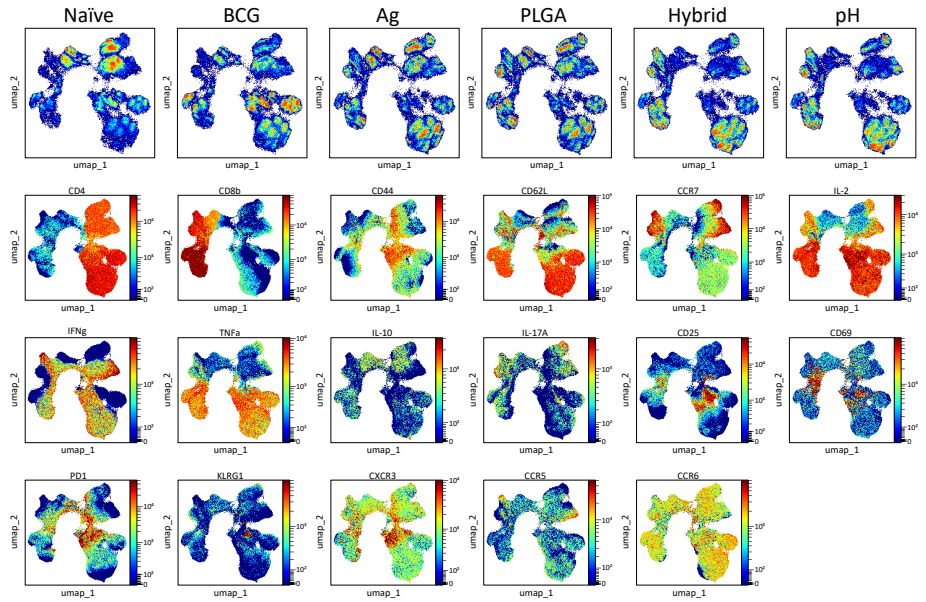


**Figure 2**. UMAP visualization of concatenated, AER-restimulated spleen-derived $CD4^+$, and $CD8^+$ T cells ($CD3^+$ $CD19^-$) from all tested mice (per group) showing differential abundances of various populations of cells followed by color-continuous plots depicting phenotypical markers distribution. Groups: naïve – unimmunized mice; BCG – live BCG; Ag –antigen (25 μg Ag85B-ESAT6-Rv2034, AER) adjuvant mix (50 μg CpG, 1 μg MPLA), NP-free; PLGA – antigen (8 μg AER) and adjuvants (2.5 μg CpG, 1 μg MPLA) delivered in PLGA (400 μg) NPs; Hybrid – antigen (8 μg AER) and adjuvants (2.5 μg CpG, 1 μg MPLA) delivered in lipid (400 μg DOPC:DOPE:DOBAQ:EPC, 3:5:2:4)-PLGA (400 μg) NPs; pH – (8 μg AER) antigen and adjuvants (2.5 μg CpG, 1 μg MPLA) delivered in cationic pH-sensitive liposomes (400 μg DOPC:DOPE:DOBAQ:EPC, 3:5:2:4).

### AER-specific $CD4^+$ and $CD8^+$ T-cell responses in splenocytes ex vivo

Splenocytes from immunized (but non-Mtb-challenged mice) were collected and restimulated with AER. The cells were then stained with a 27-color panel and analyzed using spectral flow cytometry to evaluate the immune responses. Concatenated flow cytometry events of $CD3^+$ $CD19^-$ T-cells were examined following uniform manifold approximation and projection (UMAP) dimensionality reduction (Fig. 2). UMAP was employed to evaluate global qualitative changes across experimental groups, utilizing all $CD3^+$ $CD19^-$ events simultaneously. The visual inspection of the data revealed differences in the abundance of T cells between the groups. Major differences in the abundances of $CD4^+$ and $CD8^+$ cells, especially cells expressing IL-2, IFN-γ, and TNF-α, were observed when comparing UMAPs of vaccinated mice compared to naïve mice. Subsequently, differential subset abundance analysis was performed to identify populations of interest and perform quantitative comparisons. We then selected sufficiently large cell populations (>100 events) and exhibited specific phenotypic markers that not only differentiated them from other cell subsets but also provided insights into their functional role. If several subsets were characterized by overlapping marker expression patterns, we selected one

that was defined by more markers and was still large enough. We observed several CD4⁺ T-cell subpopulations that were differentially abundant (Fig. 3). The largest population was a polyfunctional population defined as CD4⁺ IL-2⁺ IFN-γ⁺ TNF-α⁺ IL-17A⁻ IL-10⁻ CD44⁻ CD62L⁺ CCR7⁻ T cells. All AER-based vaccination groups increased this population, displaying a central memory phenotype, but interestingly, this was not the case for BCG. Similarly, a monofunctional Th1 cell subset defined as CD4⁺ IL-2⁻ IFN-γ⁺ TNF-α⁻ IL-17A⁻ IL-10⁻ CD44⁻ CD62L⁻ CCR7⁺ T cells displaying an effector memory phenotype was also differentially enriched. On the other hand, two subpopulations of CD4⁺ T cells were increased following BCG vaccination but not AER-based vaccines: a monofunctional central memory population of CD4⁺ IL-2⁺ IFN-γ⁻ TNF-α⁻ IL-17A⁻ IL-10⁻ CD44⁻ CD62L⁺ CCR7⁻ T cells as well as a population CD4⁺ IL-2⁺ TNF-α⁺ CD25⁺ CD69⁺. Th17 responses were not observed in this study.

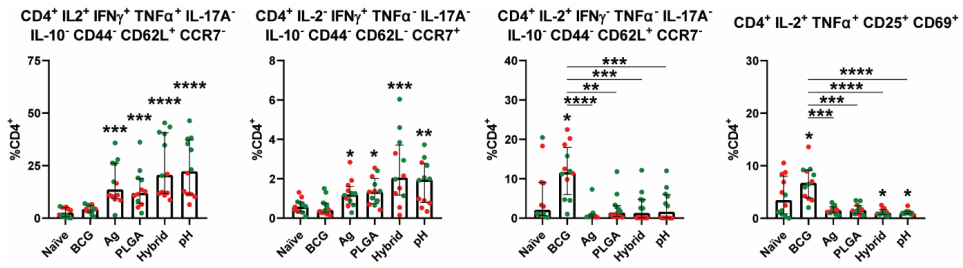


**Figure 3**. Differential abundance of CD4⁺ T-cells present in AER restimulated splenocytes from immunized non-Mtb-challenged mice. Markers defining each population are indicated above each graph. Graph values depict percentages of the population as a part of the CD3⁺ CD19⁻ CD4⁺ CD8⁻ cell subset. Each dot represents a single mouse and results from the same experiment are shown in one color. Groups: naïve – unimmunized mice; BCG – live BCG; Ag –antigen (25 μg Ag85B-ESAT6-Rv2034, AER) adjuvant mix (50 μg CpG, 1 μg MPLA), NP-free; PLGA – antigen (8 μg AER) and adjuvants (2.5 μg CpG, 1 μg MPLA) delivered in PLGA (400 μg) NPs; Hybrid – antigen (8 μg AER) and adjuvants (2.5 μg CpG, 1 μg MPLA) delivered in lipid (400 μg DOPC:DOPE:DOBAQ:EPC, 3:5:2:4)-PLGA (400 μg) NPs; pH – (8 μg AER) antigen and adjuvants (2.5 μg CpG, 1 μg MPLA) delivered in cationic pH-sensitive liposomes (400 μg DOPC:DOPE:DOBAQ:EPC, 3:5:2:4). n = 12 (mice). The minimal number of events used in the analysis was 20,000. Bars represent median ± IQR. *p < 0.05, **p< 0.01, ***p < 0.001, ****p < 0.0001 (Kruskal-Wallis with an uncorrected Dunn's posthoc test).

Similarly, we analyzed CD8⁺ T-cell populations (Fig. 4). The largest population was a polyfunctional central memory T-cell subset defined as CD8⁺ IL-2⁺ IFN-γ⁺ TNF-α⁺ IL-17A⁻ IL-10⁻ CD44⁻ CD62L⁺ CCR7⁻ T-cells. It was significantly increased in all groups immunized with AER-based vaccines but not in the case of BCG. We also observed two other subsets that were increased by AER-based vaccines: a monofunctional central memory CD4⁺ IL-2⁻ IFN-γ⁺ TNF-α⁻ IL-17A⁻ IL-10⁻ CD62L⁺ CCR7⁺ T-cells and T-cells defined as CD8⁺ IL-17A⁺ IFN-γ⁺. One population increased following BCG immunization, but none of the AER-based vaccines defined as CD8⁺ IL-2⁺ TNF-α⁺ CD44⁺ CD62L⁻ CCR7⁻ displayed predominantly an effector memory phenotype.



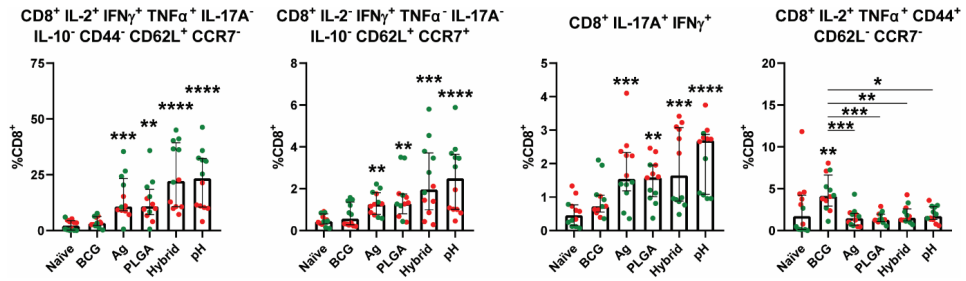


**Figure 4**. Differential abundance of CD8⁺ T-cell populations present in AER restimulated splenocytes from immunized non-Mtb-challenged mice. Markers defining each population are indicated above each graph. Graph values depict percentages of the population as a part of the CD3⁺ CD19⁻ CD4⁻ CD8⁺ cell subset. Each dot represents a percentage value from a single mouse and results from the same experiment are shown in one color. Groups: naïve – unimmunized mice; BCG – live BCG; Ag –antigen (25 μg Ag85B-ESAT6-Rv2034, AER) adjuvant mix (50 μg CpG, 1 μg MPLA), NP-free; PLGA – antigen (8 μg AER) and adjuvants (2.5 μg CpG, 1 μg MPLA) delivered in PLGA (400 μg) NPs; Hybrid – antigen (8 μg AER) and adjuvants (2.5 μg CpG, 1 μg MPLA) delivered in lipid (400 μg DOPC:DOPE:DOBAQ:EPC, 3:5:2:4)-PLGA (400 μg) NPs; pH – (8 μg AER) antigen and adjuvants (2.5 μg CpG, 1 μg MPLA) delivered in cationic pH-sensitive liposomes (400 μg DOPC:DOPE:DOBAQ:EPC, 3:5:2:4). n = 12 (mice). The minimal number of events used in the analysis was 20,000. Bars represent median ± IQR. *p < 0.05, **p< 0.01, ***p < 0.001, ****p < 0.0001 (Kruskal-Wallis with an uncorrected Dunn's posthoc test).

## Differentially abundant B-cell populations

Similar to the analysis of T-cell responses, B-cell data were dimensionally reduced and UMAPs were analyzed (Fig. 5). The UMAPs revealed the presence of differentially abundant populations of cells between different groups. Subsequently, differential subset abundance analysis was carried out, and statistically significant subsets were analyzed using univariate plots (Fig. 6). Three B-cell populations expressing activation marker CD69 were found in AER-restimulated splenocytes. The largest population was a subset identified as MHCII⁺ IgM⁻ IgD⁻ B220⁺ CD69⁺ B cells corresponding to germinal center B cells, followed by MHCII⁺ IgM⁻ IgD⁺ B220⁺ CD69⁺ (follicular B/B2 cells), and MHCII⁺ IgM⁺ IgD⁻ B220⁺ CD69⁺ (marginal zone B-cell, transitional 1 B cells) follicular B/B2) [88, 89]. All three B-cell subsets were more abundant in mouse groups vaccinated with AER-based vaccines compared to naïve mice. Moreover, mice vaccinated with lipid-PLGA hybrid NPs as well as pH-sensitive liposomes had higher counts of these B cells compared to mice vaccinated with AER mixed with CpG and MPLA. B cells defined as IL-17A⁺ B220⁺ MHCII⁺ B cells were increased in mice vaccinated with BCG compared to naïve mice and mice vaccinated with AER-based vaccines.

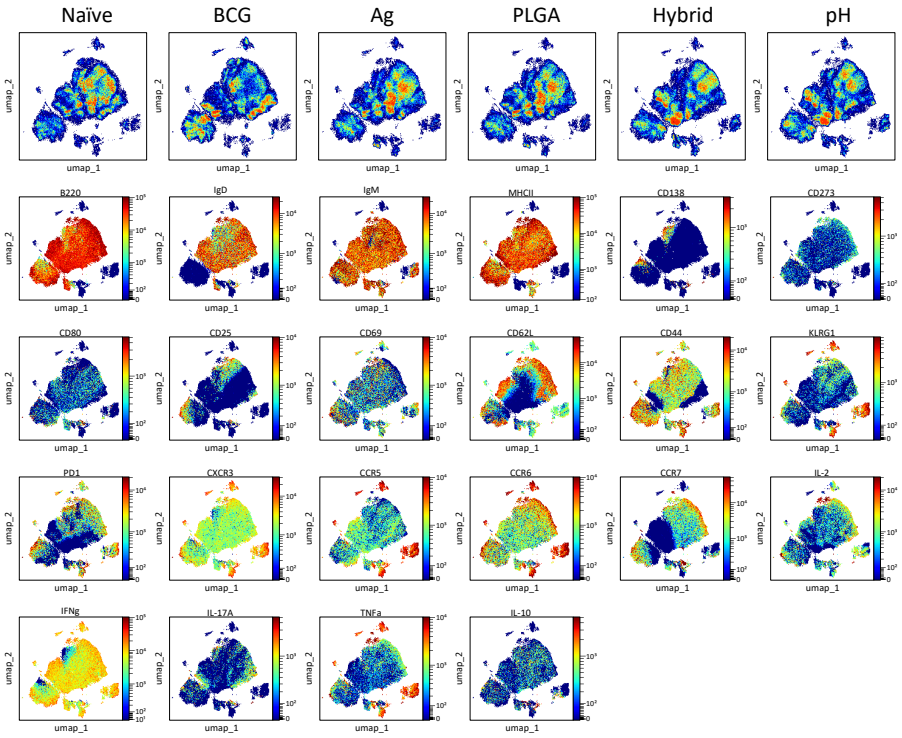


**Figure 5**. UMAP visualization of concatenated, AER-restimulated spleen-derived B-cells ($CD3^-$ $CD19^+$) from all tested mice (per group) showing differential abundances of various populations of cells followed by color-continuous plots depicting phenotypical markers distribution. Groups: naïve – unimmunized mice; BCG – live BCG; Ag –antigen (25 μg Ag85B-ESAT6-Rv2034, AER) adjuvant mix (50 μg CpG, 1 μg MPLA), NP-free; PLGA – antigen (8 μg AER) and adjuvants (2.5 μg CpG, 1 μg MPLA) delivered in PLGA (400 μg) NPs; Hybrid – antigen (8 μg AER) and adjuvants (2.5 μg CpG, 1 μg MPLA) delivered in lipid (400 μg DOPC:DOPE:DOBAQ:EPC, 3:5:2:4)-PLGA (400 μg) NPs; pH – (8 μg AER) antigen and adjuvants (2.5 μg CpG, 1 μg MPLA) delivered in cationic pH-sensitive liposomes (400 μg DOPC:DOPE:DOBAQ:EPC, 3:5:2:4).

### AER-specific antibody production

AER-specific antibody titers were investigated to explore humoral immune responses after vaccination. All four AER-based vaccines resulted in high antibody titers (Fig. 7). However, in sera from naïve and BCG-vaccinated mice, AER-specific total Ig titers were below the detection limit. The highest total as well as IgG1 and IgG2 antibody titers were observed in mice vaccinated with cationic pH-sensitive liposomes and the lowest in mice immunized with the AER-adjuvant mix. Moreover, we also observed titers of other subtypes: high IgG2b and IgG2c as well as moderate-low levels of IgG3 and IgM (Fig. S6).



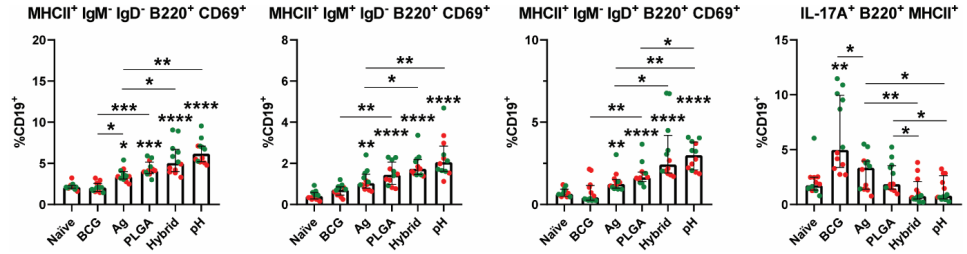


**Figure 6**. Differential abundance of $CD19^+$ B-cell populations present in AER restimulated splenocytes from immunized non-Mtb-challenged mice. Markers defining each population are indicated above each graph. Graph values depict percentages of the population as a part of the $CD3^-$ $CD19^+$ cell subset. Each dot represents a percentage value from a single mouse and results from the same experiment are shown in one color. Groups: naïve – unimmunized mice; BCG – live BCG; Ag –antigen (25 μg Ag85B-ESAT6-Rv2034, AER) adjuvant mix (50 μg CpG, 1 μg MPLA), NP-free; PLGA – antigen (8 μg AER) and adjuvants (2.5 μg CpG, 1 μg MPLA) delivered in PLGA (400 μg) NPs; Hybrid – antigen (8 μg AER) and adjuvants (2.5 μg CpG, 1 μg MPLA) delivered in lipid (400 μg DOPC:DOPE:DOBAQ:EPC, 3:5:2:4)-PLGA (400 μg) NPs; pH – (8 μg AER) antigen and adjuvants (2.5 μg CpG, 1 μg MPLA) delivered in cationic pH-sensitive liposomes (400 μg DOPC:DOPE:DOBAQ:EPC, 3:5:2:4). n = 12 (mice). The minimal number of events used in the analysis was 20,000. Bars represent median ± IQR. *$p < 0.05$, **$p < 0.01$, ***$p < 0.001$, ****$p < 0.0001$. (Kruskal-Wallis with an uncorrected Dunn's posthoc test).

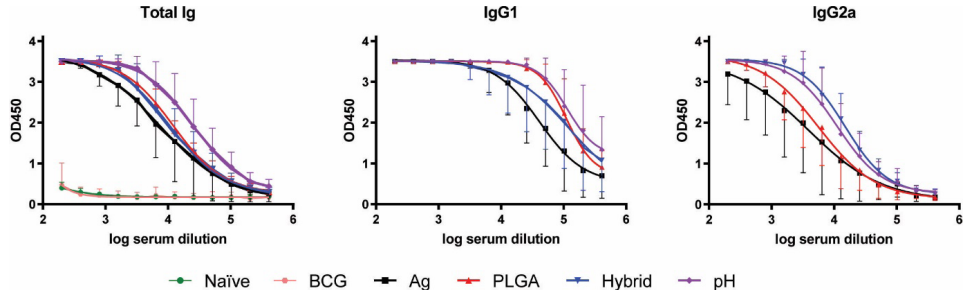


**Figure 7**. Quantification of AER-specific antibodies in sera. The type of antibody measured is indicated above each graph. Values represent OD450 ELISA, and serum dilutions are shown on the x-axis. Groups are indicated in the legend. Groups: naïve – unimmunized mice; BCG – live BCG; Ag –antigen (25 μg Ag85B-ESAT6-Rv2034, AER) adjuvant mix (50 μg CpG, 1 μg MPLA), NP-free; PLGA – antigen (8 μg AER) and adjuvants (2.5 μg CpG, 1 μg MPLA) delivered in PLGA (400 μg) NPs; Hybrid – antigen (8 μg AER) and adjuvants (2.5 μg CpG, 1 μg MPLA) delivered in lipid (400 μg DOPC:DOPE:DOBAQ:EPC, 3:5:2:4)-PLGA (400 μg) NPs; pH – (8 μg AER) antigen and adjuvants (2.5 μg CpG, 1 μg MPLA) delivered in cationic pH-sensitive liposomes (400 μg DOPC:DOPE:DOBAQ:EPC, 3:5:2:4). n = 6 (mice). Values represent mean ± standard deviation.

# DISCUSSION

TB remains a global epidemic, as a highly contagious airborne infectious disease that remains one of the foremost causes of death worldwide for centuries. According to the 2022 WHO Global Tuberculosis Report, approximately a quarter of the global population is latently infected with Mtb. Between 2000 and 2021, TB claimed the lives of 1.4 to 2 million individuals

annually, with a peak mortality between 2000 and 2010. In 2022 alone, TB was responsible for over one million deaths, surpassing fatalities from any other single infectious agent before the COVID-19 pandemic. Despite intense research efforts, the world still lacks a licensed effective TB vaccine, especially for adolescents and adults. The only licensed vaccine, BCG, offers moderate protection to infants and children but falls short for adult populations with the highest TB incidence, emphasizing the urgent need for a new vaccine [1].

NPs are very effective delivery systems for subunit vaccines, offering several advantages in enhancing their efficacy. Firstly, NPs function as adjuvants, enhancing the antigenicity of associated antigens, and can mimic some properties of pathogens like viruses. Secondly, NPs can trigger both innate and adaptive immune responses, acting as effective antigen carriers that enhance antigen processing and presentation. Their nanoscale size promotes efficient uptake by phagocytic cells and facilitates robust innate immune responses. This positions NPs as pivotal tools in next-generation vaccine development [90–92].

The physicochemical properties of NPs dictate their recognition, uptake, and immune responses [93–95]. Key properties such as size, charge, hydrophobicity, and rigidity affect interactions with interstitial matrix and antigen-presenting cells (APCs) [96, 97]. Small particles (<20 nm) drain to blood capillaries and are eliminated, while particles 20–100 nm drain into lymph nodes (LNs) and are taken up by LN-resident APCs. Larger NPs (>100 nm) remain at the injection site (SOI) until transported to LNs by resident APCs [98, 99]. Surface charge affects interactions with the interstitial matrix and cellular membranes [95]. Neutral and negatively charged NPs drain more easily into LNs [100, 101], while positively charged particles are more efficiently taken up by APCs [102, 103] and form depots, facilitating immune responses [40]. The depot effect allows precise targeting of APCs, controlled antigen release, and antigens retention at the SOI. This leads to prolonged exposure to the immune system and continuous stimulation of the APCs in the vicinity of the SOI. Rigid NPs are more efficiently taken up by APCs and facilitate depot formation at the SOI [104, 105] compared to soft NPs [106, 107]. Hydrophilic NPs may accumulate more in LNs than hydrophobic ones of similar size [108, 109].

In this study, PLGA NPs (85 nm, -50 mV) with a hydrophilic, acid-terminated surface likely exhibited short retention at the SOI and efficient transport to LNs, which resulted in strong immune responses possibly due to slow release of antigens and adjuvants from the NP core. Hybrid lipid-PLGA NPs and liposomes (140–170 nm, 20–25 mV) with hydrophilic surfaces formed palpable depots at the SOI, likely resulting in extended antigen presentation. Although hybrid NPs most likely offered a slow release of antigens and adjuvants compared to the expected burst release from liposomes, both types of NPs induced comparable protection and immune response.



To date, no clear immune correlates of protection against tuberculosis have been established. Therefore, it remains a challenge to identify types of immune responses that should be induced by a vaccine that would result in protection against Mtb. Historically, T-helper-1 responses were deemed essential for a successful TB vaccination, and this notion was supported by ample evidence [10, 110–112]. However, over time a conventional strategy aiming to induce predominant Th1/Th17 responses and minimize Th2/Treg immunity is being complemented by a more balanced approach that would lead to the interplay between Th1 and Th2 responses as well as B-cell responses. Such a diverse immune response repertoire is supposed to be more beneficial for the host.

All of the AER-containing vaccines induced primarily polyfunctional $CD4^+$ and $CD8^+$ T-cells that produced IL-2, IFN-γ, and TNF-α, as well as monofunctional IFN-γ-producing T-cells, which both displayed a central memory phenotype [113]. The observed polyfunctional T-cells expressed CD62L but not CD44 or CCR7, which could mean that they belong to a separate central memory T-cell subset that has lost CD44, as shown by Henao-Tamayo et al. [113]. $CD4^+$ T cells with such a phenotype were observed to possess a significant expansion potential and induced excellent protection when transferred to $Rag^{-/-}$ mice challenged with Mtb H37Rv but not $CD4^+$ $CD44^{hi}$ $CD62L^{lo}$ cells [114]. $CD44^{lo}$ $CD62L^{hi}$ T-cells could significantly contribute to the protective responses like T cells with $CD62L^{hi}$ $CCR7^{hi}$ central memory phenotype. Central memory $CD4^+$ T cells rather than effector memory T cells mediate long-term protection, and it has been suggested that inadequate protection conferred by BCG in adults and adolescents may be (partially) attributed to insufficient central memory T-cell responses [115].

Noteworthy, we observed a significant increase in $CD8^+$ T cells compared to naïve mice, especially in mice vaccinated with lipid-PLGA hybrid NPs, and cationic pH-sensitive liposomes. The significance of cytotoxic $CD8^+$ T cells in Mtb protection is debated. Beyond directly killing infected cells, they produce cytokines, modulate the immune response, and work together with Th1 cells [116, 117]. Recent research suggests $CD8^+$ T cells, alongside Th1 cells, are promising vaccine targets against Mtb [10, 118, 119]. Mouse studies support their importance in controlling Mtb [120–123]. Specifically, $CD8^+$ T-cell depletion increases bacterial load during latent phases in both mice [124] and non-human primates [125]. Interestingly, we observed elevated counts of IL-17A-producing $CD8^+$ T cells but not $CD4^+$ T cells. These $CD8^+$ T cells, referred to as Tc17, are postulated to exhibit functions comparable to Th17 cells [126, 127]. Th17 cells contribute to protective responses in the early stages of Mtb infection by engaging neutrophils and Th1 cells to infection sites and play a role in the formation of mature granuloma, which is crucial for the control of the disease [10, 128]. However, further investigations are necessary to elucidate the specific role of Tc17 cells in immune responses against Mtb infection.

An increase in three subsets of CD69-expressing B cells and high total AER-specific and Ig subtypes were observed in mice immunized with AER-based vaccines, which could contribute to the protection. B cell and antibody responses are believed to contribute to TB immunity, but their exact role remains ambiguous [129, 130]. Evidence for B-cell involvement is substantiated by increased vulnerability to Mtb in B-cell-depleted subjects restored post-B-cell transfer [131–133] and B-cell dysfunction in active TB patients rectifying post-treatment [134]. However, some genetic knockout studies and Mtb infection models challenge this perspective [135–137]. The protective role of antibody responses is supported by research on sera transfers from LTBI patients showing protective effects in mice [138] as well as treatment with monoclonal antibodies against Mtb antigens has been shown to improve survival, reduce spread, decrease tissue damage, and decrease mycobacterial load in animals [139–142]. Differential antibody responses between LTBI and ATB patients have also been shown. Antibodies from LTBI patients exhibited enhanced FC receptor profiles and enhanced macrophage killing of intracellular Mtb [143].

All delivery-system-based AER vaccines (PLGA, lipid-PLGA hybrid NPs, and pH-sensitive liposomes) induced protection in intranasal Mtb challenge mouse model but not AER-adjuvant mix, despite overall similar immune responses induced by all AER vaccines. Importantly, the immunological effects induced by the NP-based vaccine were achieved at significantly lower doses of the antigen and adjuvants. This highlights the substantial advantage of using these nanoparticles for vaccine delivery, as they lead to better immunological outcomes and can reduce costs associated with antigens. $CD4^+$, $CD8^+$ T-cell, and B-cell responses that we observed have been previously linked with protective outcomes by others; however, they do not explain the induced protection by these vaccines. The protection mechanism remains unknown because there are no established correlates of Mtb protection, and none of the immune responses observed in this study were associated with bacterial burden outcomes. This knowledge gap is a major hurdle in developing effective TB vaccines, and this issue has been raised in the literature before [144, 145].

The study's primary limitation is its single time point assessment, missing dynamic immune responses, and potential long-term effects. Future research should investigate multiple time points and explore various doses of the antigen, NPs, and adjuvants. The 7-day lymphocyte restimulation limited early immune responses study. The lack of immune response data from Mtb-challenged mice limits direct protection correlation. However, the study's strength lies in linking human innate responses with adaptive immune responses in vaccinated mice, finding NP-based vaccines that outperform BCG, hinting at broader applicability to other models and human use.



# CONCLUSION

In this study, three types of NP-based potential TB vaccines were compared *in vivo*: PLGA, lipid-PLGA hybrid NPs, and cationic pH-sensitive liposomes. The formulations used Ag85B-ESAT6-Rv2034 AER fusion antigen, and two adjuvants (CpG and MPLA). Lipids used in the production of the hybrid NPs and liposomes comprised of DOPC:DOPE:DOBAQ:EPC at 3:5:2:4 molar ratio. This study describes the side-by-side comparison of three types of delivery systems in terms of protection (Mtb burden reduction in lungs and spleens) as well as a comprehensive exploration of immune responses: $CD4^+$/$CD8^+$ T-cell, B-cell, and antigen-specific antibody production. Vaccines that used NP-based delivery systems induced protection in intranasal Mtb-challenged mice as indicated by a significant CFU reduction compared to NP-free vaccination (AER mixed with CpG and MPLA). Moreover, NP-based vaccines induced a significant increase in polyfunctional $CD4^+$, and $CD8^+$ T-cells, as well as $CD69^+$ B-cell subsets, and high antigen-specific antibody titers. NP-based vaccines induced protection and protective immune responses at much lower doses of the antigen and molecular adjuvants than the NP-free vaccine. Our study's strength lies in linking human innate with adaptive immune responses in immunized mice, thereby identifying NP-based vaccines that outperform BCG. PLGA, lipid-PLGA hybrid NPs, and cationic pH-sensitive liposomes are excellent promising vaccine delivery candidates, and their application should be further explored.

## References


1. World Health Organization, 2023. Global Tuberculosis Report 2023. Geneva. https://iris.who.int/handle/10665/373828.
2. Coppola, M., Ottenhoff, T.H., 2018. Genome wide approaches discover novel Mycobacterium tuberculosis antigens as correlates of infection, disease, immunity and targets for vaccination. Semin. Immunol. 39, 88–101. https://doi.org/10.1016/J.SMIM.2018.07.001.
3. World Health Organization, 2015. The end TB strategy. World Health Organization, https://iris.who.int/handle/10665/331326.
4. World Health Organization, 2015. Implementing the end TB strategy: the essentials. World Health Organization, https://iris.who.int/handle/10665/206499.
5. World Health Organization, 2022a. Western Pacific regional framework to end TB: 2021-2030. WHO Regional Office for the Western Pacific, https://iris.who.int/handle/10665/352278.
6. Pérez-Alós, L., Armenteros, J.J.A., Madsen, J.R., Hansen, C.B., Jarlhelt, I., Hamm, S.R., Heftdal, L.D., Pries-Heje, M.M., Møller, D.L., Fogh, K., Hasselbalch, R.B., Rosbjerg, A., Brunak, S., Sørensen, E., Larsen, M.A.H., Ostrowski, S.R., Frikke-Schmidt, R., Bayarri-Olmos, R., Hilsted, L.M., Iversen, K.K., Bundgaard, H., Nielsen, S.D., Garred, P., 2022. Modeling of waning immunity after SARS-CoV-2 vaccination and influencing factors. Nat. Commun. 2022 13:1 13, 1–11. https://doi.org/10.1038/s41467-022-29225-4.
7. Pollard, A.J., Bijker, E.M., 2020. A guide to vaccinology: from basic principles to new developments. Nat. Rev. Immunol. 2020 21:2 21, 83–100. https://doi.org/10.1038/s41577-020-00479-7.
8. Rémy, V., Zöllner, Y., Heckmann, U., 2015. Vaccination: the cornerstone of an efficient healthcare system. J. Mark. Access Health Policy 3, 27041. https://doi.org/10.3402/JMAHP.V3.27041.
9. Brewer, T.F., 2000. Preventing Tuberculosis with Bacillus Calmette-Guérin Vaccine: A Meta-Analysis of the Literature. Clin. Infect. Dis. 31, S64–S67. https://doi.org/10.1086/314072.
10. Ottenhoff, T.H.M., Kaufmann, S.H.E., 2012. Vaccines against Tuberculosis: Where Are We and Where Do We Need to Go? PLoS Pathog. 8, e1002607. https://doi.org/10.1371/journal.ppat.1002607.
11. Trunz, B.B., Fine, P., Dye, C., 2006. Effect of BCG vaccination on childhood tuberculous meningitis and miliary tuberculosis worldwide: a meta-analysis and assessment of cost-effectiveness. Lancet 367, 1173–1180. https://doi.org/10.1016/S0140-6736(06)68507-3.
12. Christensen, D., Korsholm, K.S., Andersen, P., Agger, E.M., 2011. Cationic liposomes as vaccine adjuvants. Expert Rev. Vaccines 10, 513–521. https://doi.org/10.1586/erv.11.17.
13. Moyle, P.M., Toth, I., 2013. Modern Subunit Vaccines: Development, Components, and Research Opportunities. ChemMedChem 8, 360–376. https://doi.org/10.1002/cmdc.201200487.
14. Barnier-Quer, C., Elsharkawy, A., Romeijn, S., Kros, A., Jiskoot, W., 2013. Adjuvant Effect of Cationic Liposomes for Subunit Influenza Vaccine: Influence of Antigen Loading Method, Cholesterol and Immune Modulators. Pharmaceutics 5, 392–410. https://doi.org/10.3390/pharmaceutics5030392.
15. Tandrup Schmidt, S., Foged, C., Smith Korsholm, K., Rades, T., Christensen, D., 2016. Liposome-Based Adjuvants for Subunit Vaccines: Formulation Strategies for Subunit Antigens and Immunostimulators. Pharmaceutics 8, 7. https://doi.org/10.3390/pharmaceutics8010007.
16. Marasini, N., Ghaffar, K.A., Skwarczynski, M., Toth, I., 2017. Liposomes as a Vaccine Delivery System, in: Micro- and Nanotechnology in Vaccine Development, 221–239. https://doi.org/10.1016/B978-0-323-39981-4.00012-9.
17. Silva, A.L., Soema, P.C., Slütter, B., Ossendorp, F., Jiskoot, W., 2016. PLGA particulate delivery systems for subunit vaccines: Linking particle properties to immunogenicity. Hum. Vaccin. Immunother. 12, 1056–1069. https://doi.org/10.1080/21645515.2015.1117714.
18. Storni, T., Kündig, T.M., Senti, G., Johansen, P., 2005. Immunity in response to particulate antigen-delivery systems. Adv. Drug Deliv. Rev. 57, 333–355. https://doi.org/10.1016/J.ADDR.2004.09.008.
19. Allahyari, M., Mohit, E., 2016. Peptide/protein vaccine delivery system based on PLGA particles. Hum. Vaccin. Immunother. 12, 806–828. https://doi.org/10.1080/21645515.2015.1102804.
20. Danhier, F., Ansorena, E., Silva, J.M., Coco, R., Le Breton, A., Préat, V., 2012. PLGA-based nanoparticles: An overview of biomedical applications. J. Control. Release 161, 505–522. https://doi.org/10.1016/J.JCONREL.2012.01.043.
21. Duong, V.T., Skwarczynski, M., Toth, I., 2023. Towards the development of subunit vaccines against tuberculosis: The key role of adjuvant. Tuberculosis 139, 102307. https://doi.org/10.1016/J.TUBE.2023.102307.
22. Ignjatovic, N.L., Ajdukovic, Z.R., Savic, V.P., Uskokovic, D.P., 2010. Size effect of calcium phosphate coated with poly-DL-lactide-co-glycolide on healing processes in bone reconstruction. J. Biomed. Mater. Res. B. Appl. Biomater. 94B, 108–117. https://doi.org/10.1002/JBM.B.31630.
23. Jain, R.A., 2000. The manufacturing techniques of various drug loaded biodegradable poly(lactide-co-glycolide) (PLGA) devices. Biomaterials 21, 2475–2490. https://doi.org/10.1016/S0142-9612(00)00115-0.
24. Lü, J.M., Wang, X., Marin-Muller, C., Wang, H., Lin, P.H., Yao, Q., Chen, C., 2014. Current advances in research and clinical applications of PLGA-based nanotechnology. Expert Rev. Mol. Diagn. 9, 325–341. https://doi.org/10.1586/ERM.09.15.
25. Akagi, T., Baba, M., Akashi, M., 2012. Biodegradable nanoparticles as vaccine adjuvants and delivery systems: Regulation of immune responses by nanoparticle-based vaccine. Adv. Polym. Sci. 247, 31–64. https://doi.org/10.1007/12_2011_150.
26. Ashhurst, A.S., Parumasivam, T., Chan, J.G.Y., Lin, L.C.W., Flórido, M., West, N.P., Chan, H.K., Britton, W.J., 2018. PLGA particulate subunit tuberculosis vaccines promote humoral and Th17 responses but do not enhance control of Mycobacterium tuberculosis infection. PLoS One 13, e0194620. https://doi.org/10.1371/JOURNAL.PONE.0194620.
27. Chong, C.S.W., Cao, M., Wong, W.W., Fischer, K.P., Addison, W.R., Kwon, G.S., Tyrrell, D.L., Samuel, J., 2005. Enhancement of T helper type 1 immune responses against hepatitis B virus core antigen by PLGA nanoparticle vaccine delivery. J. Control. Release 102, 85–99. https://doi.org/10.1016/J.JCONREL.2004.09.014.
28. Hamdy, S., Molavi, O., Ma, Z., Haddadi, A., Alshamsan, A., Gobti, Z., Elhasi, S., Samuel, J., Lavasanifar, A., 2008. Co-delivery of cancer-associated antigen and Toll-like receptor 4 ligand in PLGA nanoparticles induces potent CD8+ T cell-mediated anti-tumor immunity. Vaccine 26, 5046–5057. https://doi.org/10.1016/J.VACCINE.2008.07.035.
29. Liang, Z., Li, M., Ni, J., Hussain, T., Yao, J., Song, Y., Liu, Y., Wang, H., Zhou, X., 2022. CFP10–loaded PLGA nanoparticles as a booster vaccine confer protective immunity against Mycobacterium bovis. Bioimpacts 12, 395. https://doi.org/10.34172/BI.2022.23645.
30. Malik, A., Gupta, M., Mani, R., Bhatnagar, R., 2019. Single-dose Ag85b-ESAT6–loaded poly(Lactic-co-glycolic acid) nanoparticles confer protective immunity against tuberculosis. Int. J. Nanomedicine 14, 3129–3143. https://doi.org/10.2147/IJN.S172391.
31. Ni, J., Liu, Y., Hussain, T., Li, M., Liang, Z., Liu, T., Zhou, X., 2021. Recombinant ArgF PLGA nanoparticles enhances BCG induced immune responses against Mycobacterium bovis infection. Biomed. Pharmacother.137, 111341. https://doi.org/10.1016/J.BIOPHA.2021.111341.
32. Schlosser, E., Mueller, M., Fischer, S., Basta, S., Busch, D.H., Gander, B., Groettrup, M., 2008. TLR ligands and antigen need to be coencapsulated into the same biodegradable microsphere for the generation of potent cytotoxic T lymphocyte responses. Vaccine 26, 1626–1637. https://doi.org/10.1016/J.VACCINE.2008.01.030.
33. Heuts, J., Varypataki, E.M., van der Maaden, K., Romeijn, S., Drijfhout, J.W., van Scheltinga, A.T., Ossendorp, F., Jiskoot, W., 2018. Cationic Liposomes: A Flexible Vaccine Delivery System for Physicochemically Diverse Antigenic Peptides. Pharm. Res. 35, 1–9. https://doi.org/10.1007/s11095-018-2490-6.
34. Latif, N., Bachhawat, B.K., 1984. The effect of surface charges of liposomes in immunopotentiation. Biosci. Rep. 4, 99–107. https://doi.org/10.1007/BF01120305.
35. Liu, X., Da, Z., Wang, Yue, Niu, H., Li, R., Yu, H., He, S., Guo, M., Wang, Yong, Luo, Y., Ma, X., Zhu, B., 2016. A novel liposome adjuvant DPC mediates Mycobacterium tuberculosis subunit vaccine well to induce cell-mediated immunity and high protective efficacy in mice. Vaccine 34, 1370–1378. https://doi.org/10.1016/j.vaccine.2016.01.049.
36. Khademi, F., Taheri, R.A., Momtazi-Borojeni, A.A., Farnoosh, G., Johnston, T.P., Sahebkar, A., 2018. Potential of cationic liposomes as adjuvants/delivery systems for tuberculosis subunit vaccines, in: Reviews of Physiology, Biochemistry and Pharmacology, 47–69. https://doi.org/10.1007/112_2018_9.
37. Luwi, N.E.M., Ahmad, S., Azlyna, A.S.N., Nordin, A., Sarmiento, M.E., Acosta, A., Azmi, M.N., Uskoković, V., Mohamud, R., Kadir, R.,

2022. Liposomes as immunological adjuvants and delivery systems in the development of tuberculosis vaccine: A review. Asian Pac. J. Trop. Med. https://doi.org/10.4103/1995-7645.332806.
38. Tretiakova, D.S., Vodovozova, E.L., 2022. Liposomes as Adjuvants and Vaccine Delivery Systems. Biochem. (Mosc.) Suppl. Ser. A Membr. Cell Biol. 16:1 16, 1–20. https://doi.org/10.1134/S1990747822020076.
39. Du, G., Hathout, R.M., Nasr, M., Nejadnik, M.R., Tu, J., Koning, R.I., Koster, A.J., Slütter, B., Kros, A., Jiskoot, W., Bouwstra, J.A., Mönkäre, J., 2017. Intradermal vaccination with hollow figure needles: A comparative study of various protein antigen and adjuvant encapsulated nanoparticles. J. Control. Release 266, 109–118. https://doi.org/10.1016/j.jconrel.2017.09.021.
40. Henriksen-Lacey, M., Bramwell, V.W., Christensen, D., Agger, E.M., Andersen, P., Perrie, Y., 2010. Liposomes based on dimethyldioctadecylammonium promote a depot effect and enhance immunogenicity of soluble antigen. J. Control. Release 142, 180–186. https://doi.org/10.1016/j.jconrel.2009.10.022.
41. Nakanishi, T., Kunisawa, J., Hayashi, A., Tsutsumi, Y., Kubo, K., Nakagawa, S., Nakanishi, M., Tanaka, K., Mayumi, T., 1999. Positively charged liposome functions as an efficient immunoadjuvant in inducing cell-mediated immune response to soluble proteins. J. Control. Release 61, 233–240. https://doi.org/10.1016/S0168-3659(99)00097-8.
42. Balamurali, V., Pramodkuma, T.M., Srujana, N., Venkatesh, M.P., Gupta, N.V., Krishna, K.L., Gangadhara, H.V., 2010. pH Sensitive Drug Delivery Systems: A Review. Am. J. Drug Discov. Dev. 1, 24–48. https://doi.org/10.3923/AJDD.2011.24.48.
43. Karanth, H., Murthy, R.S.R., 2007. pH-Sensitive liposomes-principle and application in cancer therapy. J. Pharm. Pharmacol. 59, 469–483. https://doi.org/10.1211/JPP.59.4.0001.
44. Liu, X., Huang, G., 2013. Formation strategies, mechanism of intracellular delivery and potential clinical applications of pH-sensitive liposomes. Asian J. Pharm. Sci. 8, 319–328. https://doi.org/10.1016/J.AJPS.2013.11.002.
45. Mu, Y., Gong, L., Peng, T., Yao, J., Lin, Z., 2021. Advances in pH-responsive drug delivery systems. OpenNano 5, 100031. https://doi.org/10.1016/J.ONANO.2021.100031.
46. Zhuo, S., Zhang, F., Yu, J., Zhang, X., Yang, G., Liu, X., 2020. pH-Sensitive Biomaterials for Drug Delivery. Molecules 25. https://doi.org/10.3390/MOLECULES25235649.
47. Chang, J.S., Choi, M.J., Cheong, H.S., Kim, K., 2001. Development of Th1-mediated CD8+ effector T cells by vaccination with epitope peptides encapsulated in pH-sensitive liposomes. Vaccine 19, 3608–3614. https://doi.org/10.1016/S0264-410X(01)00104-9.
48. Andersen, B.M., Ohlfest, J.R., 2012. Increasing the efficacy of tumor cell vaccines by enhancing cross priming. Cancer Lett. 325, 155–164. https://doi.org/10.1016/J.CANLET.2012.07.012.
49. Fehres, C.M., Unger, W.W.J., Garcia-Vallejo, J.J., van Kooyk, Y., 2014. Understanding the biology of antigen cross-presentation for the design of vaccines against cancer. Front. Immunol. 5, 149. https://doi.org/10.3389/FIMMU.2014.00149.
50. Melero, I., Gaudernack, G., Gerritsen, W., Huber, C., Parmiani, G., Scholl, S., Thatcher, N., Wagstaff, J., Zielinski, C., Faulkner, I., Mellstedt, H., 2014. Therapeutic vaccines for cancer: an overview of clinical trials. Nat. Rev. Clin. Oncol. 11:9, 509–524. https://doi.org/10.1038/nrclinonc.2014.111.
51. Wang, C., Li, P., Liu, L., Pan, H., Li, H., Cai, L., Ma, Y., 2016. Self-adjuvanted nanovaccine for cancer immunotherapy: Role of lysosomal rupture-induced ROS in MHC class I antigen presentation. Biomaterials 79, 88–100. https://doi.org/10.1016/J.BIOMATERIALS.2015.11.040.
52. Alsaab, H.O., Alharbi, F.D., Alhibs, A.S., Alanazi, N.B., Alshehri, B.Y., Saleh, M.A., Alshehri, F.S., Algarni, M.A., Almugaiteeb, T., Uddin, M.N., Alzhrani, R.M., 2022. PLGA-Based Nanomedicine: History of Advancement and Development in Clinical Applications of Multiple Diseases. Pharmaceutics 14:12, 2728. https://doi.org/10.3390/PHARMACEUTICS14122728.
53. Hadinoto, K., Sundaresan, A., Cheow, W.S., 2013. Lipid–polymer hybrid nanoparticles as a new generation therapeutic delivery platform: A review. Eur. J. Pharm. Biopharm. 85, 427–443. https://doi.org/10.1016/J.EJPB.2013.07.002.
54. Pandita, D., Kumar, S., Lather, V., 2015. Hybrid poly(lactic-co-glycolic acid) nanoparticles: design and delivery prospectives. Drug Discov. Today 20, 95–104. https://doi.org/10.1016/J.DRUDIS.2014.09.018.
55. Sah, H., Thoma, L.A., Desu, H.R., Sah, E., Wood, G.C., 2013. Concepts and practices used to develop functional PLGA-based nanoparticulate systems. Int. J. Nanomedicine 8, 747–765. https://doi.org/10.2147/IJN.S40579.
56. Tan, S., Li, X., Guo, Y., Zhang, Z., 2013. Lipid-enveloped hybrid nanoparticles for drug delivery. Nanoscale 5, 860–872. https://doi.org/10.1039/C2NR32880A.
57. Ghitman, J., Biru, E.I., Stan, R., Iovu, H., 2020. Review of hybrid PLGA nanoparticles: Future of smart drug delivery and theranostics medicine. Mater. Des. 193, 108805. https://doi.org/10.1016/J.MATDES.2020.108805.
58. Rose, F., Wern, J.E., Ingvarsson, P.T., Van De Weert, M., Andersen, P., Follmann, F., Foged, C., 2015. Engineering of a novel adjuvant based on lipid-polymer hybrid nanoparticles: A quality-by-design approach. J. Control. Release 210, 48–57. https://doi.org/10.1016/J.JCONREL.2015.05.004.
59. Khademi, F., Derakhshan, M., Yousefi-Avarvand, A., Najafi, A., Tafaghodi, M., 2018. A novel antigen of Mycobacterium tuberculosis and MPLA adjuvant co-entrapped into PLGA:DDA hybrid nanoparticles stimulates mucosal and systemic immunity. Microb. Pathog. 125, 507–513. https://doi.org/10.1016/J.MICPATH.2018.10.023.
60. Khademi, F., Sahebkar, A., Fasihi-Ramandi, M., Taheri, R.A., 2018. Induction of strong immune response against a multicomponent antigen of Mycobacterium tuberculosis in BALB/c mice using PLGA and DOTAP adjuvant. APMIS 126, 509–514. https://doi.org/10.1111/APM.12851.
61. Liu, L., Cao, F., Liu, X., Wang, H., Zhang, C., Sun, H., Wang, C., Leng, X., Song, C., Kong, D., Ma, G., 2016. Hyaluronic Acid-Modified Cationic Lipid-PLGA Hybrid Nanoparticles as a Nanovaccine Induce Robust Humoral and Cellular Immune Responses. ACS Appl. Mater. Interfaces 8, 11969–11979. https://doi.org/https://doi.org/10.1021/acsami.6b01135.
62. Liu, L., Ma, P., Wang, H., Zhang, C., Sun, H., Wang, C., Song, C., Leng, X., Kong, D., Ma, G., 2016. Immune responses to vaccines delivered by encapsulation into and/or adsorption onto cationic lipid-PLGA hybrid nanoparticles. J. Control. Release 225, 230–239. https://doi.org/10.1016/J.JCONREL.2016.01.050.
63. Moon, J.J., Suh, H., Polhemus, M.E., Ockenhouse, C.F., Yadava, A., Irvine, D.J., 2012. Antigen-Displaying Lipid-Enveloped PLGA Nanoparticles as Delivery Agents for a Plasmodium vivax Malaria Vaccine. PLoS One 7, e31472. https://doi.org/10.1371/JOURNAL.PONE.0031472.
64. Rose, F., Wern, J.E., Gavins, F., Andersen, P., Follmann, F., Foged, C., 2018. A strong adjuvant based on glycol-chitosan-coated lipid-polymer hybrid nanoparticles potentiates mucosal immune responses against the recombinant Chlamydia trachomatis fusion antigen CTH522. J. Control. Release 271, 88–97. https://doi.org/10.1016/J.JCONREL.2017.12.003.
65. Karbalaei Zadeh Babaki, M., Soleimanpour, S., Rezaee, S.A., 2017. Antigen 85 complex as a powerful Mycobacterium tuberculosis immunogene: Biology, immune-pathogenicity, applications in diagnosis, and vaccine design. Microb. Pathog. 112, 20–29. https://doi.org/10.1016/J.MICPATH.2017.08.040.
66. Li, W., Deng, G., Li, M., Zeng, J., Zhao, L., Liu, X., Wang, Y., 2014. A recombinant adenovirus expressing CFP10, ESAT6, Ag85A and Ag85B of Mycobacterium tuberculosis elicits strong antigen-specific immune responses in mice. Mol. Immunol. 62, 86–95. https://doi.org/10.1016/J.MOLIMM.2014.06.007.
67. Mearns, H., Geldenhuys, H.D., Kagina, B.M., Musvosvi, M., Little, F., Ratangee, F., Mahomed, H., Hanekom, W.A., Hoff, S.T., Ruhwald, M., Kromann, I., Bang, P., Hatherill, M., Andersen, P., Scriba, T.J., Rozot, V., Abrahams, D.A., Mauff, K., Smit, E., Brown, Y., Hughes, E.J., Makgotlho, E., Keyser, A., Erasmus, M., Makhethe, L., Africa, H., Hopley, C., Steyn, M., 2017. H1:IC31 vaccination is safe and induces long-lived TNF-α+IL-2+CD4 T cell responses in M. tuberculosis infected and uninfected adolescents: A randomized trial. Vaccine 35, 132–141. https://doi.org/10.1016/J.VACCINE.2016.11.023.
68. Luabeya, A.K.K., Kagina, B.M.N., Tameris, M.D., Geldenhuys, H., Hoff, S.T., Shi, Z., Kromann, I., Hatherill, M., Mahomed, H., Hanekom, W.A., Andersen, P., Scriba, T.J., Schoeman, E., Krohn, C., Day, C.L., Africa, H., Makhethe, L., Smit, E., Brown, Y., Suliman, S., Hughes, E.J., Bang, P., Snowden, M.A., McClain, B., Hussey, G.D., 2015. First-in-human trial of the post-exposure tuberculosis vaccine H56:IC31 in Mycobacterium tuberculosis infected and non-infected healthy adults. Vaccine 33, 4130–4140. https://doi.org/10.1016/J.VACCINE.2015.06.051.
69. Commandeur, S., van Meijgaarden, K.E., Prins, C., Pichugin, A. V., Dijkman, K., van den Eeden, S.J.F., Friggen, A.H., Franken, K.L.M.C., Dolganov, G., Kramnik, I., Schoolnik, G.K., Oftung, F., Korsvold, G.E., Geluk, A., Ottenhoff, T.H.M., 2013. An Unbiased Genome-Wide Mycobacterium tuberculosis Gene Expression Approach To Discover Antigens Targeted by

Human T Cells Expressed during Pulmonary Infection. J. Immunol. 190, 1659–1671. https://doi.org/10.4049/JIMMUNOL.1201593.
70. Commandeur, S., van den Eeden, S.J.F., Dijkman, K., Clark, S.O., van Meijgaarden, K.E., Wilson, L., Franken, K.L.M.C., Williams, A., Christensen, D., Ottenhoff, T.H.M., Geluk, A., 2014. The in vivo expressed Mycobacterium tuberculosis (IVE-TB) antigen Rv2034 induces CD4+ T-cells that protect against pulmonary infection in HLA-DR transgenic mice and guinea pigs. Vaccine 32, 3580–3588. https://doi.org/10.1016/j.vaccine.2014.05.005.
71. Ko, E.J., Lee, Y., Lee, Y.T., Kim, Y.J., Kim, K.H., Kang, S.M., 2018. MPL and CpG combination adjuvants promote homologous and heterosubtypic cross protection of inactivated split influenza virus vaccine. Antiviral Res. 156, 107–115. https://doi.org/10.1016/J.ANTIVIRAL.2018.06.004.
72. Meraz, I.M., Savage, D.J., Segura-Ibarra, V., Li, J., Rhudy, J., Gu, J., Serda, R.E., 2014. Adjuvant cationic liposomes presenting MPL and IL-12 induce cell death, suppress tumor growth, and alter the cellular phenotype of tumors in a murine model of breast cancer. Mol. Pharm. 11, 3484–3491. https://doi.org/10.1021/mp5002697.
73. Todoroff, J., Lemaire, M.M., Fillee, C., Jurion, F., Renauld, J.C., Huygen, K., Vanbever, R., 2013. Mucosal and Systemic Immune Responses to Mycobacterium tuberculosis Antigen 85A following Its Co-Delivery with CpG, MPLA or LTB to the Lungs in Mice. PLoS One 8, e63344. https://doi.org/10.1371/JOURNAL.PONE.0063344.
74. Dreno, B., Thompson, J.F., Smithers, B.M., Santinami, M., Jouary, T., Gutzmer, R., Levchenko, E., Rutkowski, P., Grob, J.J., Korovin, S., Drucis, K., Grange, F., Machet, L., Hersey, P., Krajsova, I., Testori, A., Conry, R., Guillot, B., Kruit, W.H.J., Demidov, L., Thompson, J.A., Bondarenko, I., Jaroszek, J., Puig, S., Cinat, G., Hauschild, A., Goeman, J.J., van Houwelingen, H.C., Ulloa-Montoya, F., Callegaro, A., Dizier, B., Spiessens, B., Debois, M., Brichard, V.G., Louahed, J., Therasse, P., Debruyne, C., Kirkwood, J.M., 2018. MAGE-A3 immunotherapeutic as adjuvant therapy for patients with resected, MAGE-A3-positive, stage III melanoma (DERMA): a double-blind, randomised, placebo-controlled, phase 3 trial. Lancet Oncol. 19, 916–929. https://doi.org/10.1016/S1470-2045(18)30254-7.
75. Gutzmer, R., Rivoltini, L., Levchenko, E., Testori, A., Utikal, J., Ascierto, P.A., Demidov, L., Grob, J.J., Ridolfi, R., Schadendorf, D., Queirolo, P., Santoro, A., Loquai, C., Dreno, B., Hauschild, A., Schultz, E., Lesimple, T.P., Vanhoutte, N., Salaun, B., Gillet, M., Jarnjak, S., De Sousa Alves, P.M., Louahed, J., Brichard, V.G., Lehmann, F.F., 2016. Safety and immunogenicity of the PRAME cancer immunotherapeutic in metastatic melanoma: results of a phase I dose escalation study. ESMO Open 1, e000068. https://doi.org/10.1136/ESMOOPEN-2016-000068.
76. Kruit, W.H., Suciu, S., Dreno, B., Chiarion-Sileni, V., Mortier, L., Robert, C., Maio, M., Brichard, V.G., Lehmann, F., Keilholz, U., 2008. Immunization with recombinant MAGE-A3 protein combined with adjuvant systems AS15 or AS02B in patients with unresectable and progressive metastatic cutaneous melanoma: A randomized open-label phase II study of the EORTC Melanoma Group (16032- 18031). J. Clin. Oncol. 26, 9065–9065. https://doi.org/10.1200/JCO.2008.26.15_SUPPL.9065.
77. Kruit, W.H.J., Suciu, S., Dreno, B., Mortier, L., Robert, C., Chiarion-Sileni, V., Maio, M., Testori, A., Dorval, T., Grob, J.J., Becker, J.C., Spatz, A., Eggermont, A.M.M., Louahed, J., Lehmann, F.F., Brichard, V.G., Keilholz, U., 2013. Selection of immunostimulant AS15 for active immunization with MAGE-A3 protein: results of a randomized phase II study of the European Organisation for Research and Treatment of Cancer Melanoma Group in Metastatic Melanoma. J. Clin. Oncol. 31, 2413–2420. https://doi.org/10.1200/JCO.2012.43.7111.
78. Vansteenkiste, J.F., Cho, B.C., Vanakesa, T., De Pas, T., Zielinski, M., Kim, M.S., Jassem, J., Yoshimura, M., Dahabreh, J., Nakayama, H., Havel, L., Kondo, H., Mitsudomi, T., Zarogoulidis, K., Gladkov, O.A., Udud, K., Tada, H., Hoffman, H., Bugge, A., Taylor, P., Gonzalez, E.E., Liao, M.L., He, J., Pujol, J.L., Louahed, J., Debois, M., Brichard, V., Debruyne, C., Therasse, P., Altorki, N., 2016. Efficacy of the MAGE-A3 cancer immunotherapeutic as adjuvant therapy in patients with resected MAGE-A3-positive non-small-cell lung cancer (MAGRIT): a randomised, double-blind, placebo-controlled, phase 3 trial. Lancet Oncol. 17, 822–835. https://doi.org/10.1016/S1470-2045(16)00099-1.
79. Franken, K.L.M.C., Hiemstra, H.S., Van Meijgaarden, K.E., Subronto, Y., Den Hartigh, J., Ottenhoff, T.H.M., Drijfhout, J.W., 2000. Purification of His-Tagged Proteins by Immobilized Chelate Affinity Chromatography: The Benefits from the Use of Organic Solvent. Protein Expr. Purif. 18, 95–99. https://doi.org/10.1006/PREP.1999.1162.
80. Szachniewicz, M.M., Neustrup, M.A., van Meijgaarden, K.E., Jiskoot, W., Bouwstra, J.A., Haks, M.C., Geluk, A., Ottenhoff, T.H.M., 2024. Intrinsic immunogenicity of liposomes for tuberculosis vaccines: Effect of cationic lipid and cholesterol. Eur. J. Pharm. Sci. 195, 106730. https://doi.org/10.1016/J.EJPS.2024.106730.
81. Verreck, F.A.W., Boer, T. de, Langenberg, D.M.L., Zanden, L. van der, Ottenhoff, T.H.M., 2006. Phenotypic and functional profiling of human proinflammatory type-1 and anti-inflammatory type-2 macrophages in response to microbial antigens and IFN-γ- and CD40L-mediated costimulation. J. Leukoc. Biol. 79, 285–293. https://doi.org/10.1189/JLB.0105015.
82. Szachniewicz, M.M., van Meijgaarden, K.E., Kavrik, E., Jiskoot, W., Bouwstra, J.A., Haks, M.C., Geluk, A., Ottenhoff, T.H.M., 2024. Cationic pH-sensitive liposomes as subunit vaccine delivery systems against tuberculosis: effect of liposome composition on cellular innate immune responses. Int. Immunopharmacol. Manuscript submitted for publication.
83. Szachniewicz, M.M., van den Eeden, S.J.F., van Meijgaarden, K.E., Franken, K.L.M.C., van Veen, S., Geluk, A., Bouwstra, J.A., Ottenhoff, T.H.M., 2024. Cationic pH-sensitive liposome-based subunit tuberculosis vaccine induces protection in mice challenged with Mycobacterium tuberculosis. Eur. J. Pharm. Biopharm. 203, 114437. https://doi.org/10.1016/J.EJPB.2024.114437.
84. Geluk, A., van den Eeden, S.J.F., van Meijgaarden, K.E., Dijkman, K., Franken, K.L.M.C., Ottenhoff, T.H.M., 2012. A multistage-polyepitope vaccine protects against Mycobacterium tuberculosis infection in HLA-DR3 transgenic mice. Vaccine 30, 7513–7521. https://doi.org/10.1016/J.VACCINE.2012.10.045.
85. Ali, M., van Gent, M.E., de Waal, A.M., van Doodewaerd, B.R., Bos, E., Koning, R.I., Cordfunke, R.A., Drijfhout, J.W., Nibbering, P.H., 2023. Physical and Functional Characterization of PLGA Nanoparticles Containing the Antimicrobial Peptide SAAP-148. Int. J. Mol. Sci. 24, 2867. https://doi.org/10.3390/IJMS24032867/S1.
86. R Core Team, 2023. R: A language and environment for statistical computing.
87. RStudio Team, 2023. RStudio: Integrated Development Environment for R.
88. Kleiman, E., Salyakina, D., De Heusch, M., Hoek, K.L., Llanes, J.M., Castro, I., Wright, J.A., Clark, E.S., Dykxhoorn, D.M., Capobianco, E., Takeda, A., Renauld, J.C., Khan, W.N., 2015. Distinct transcriptomic features are associated with transitional and mature B-cell populations in the mouse spleen. Front. Immunol. 6, 126060. https://doi.org/10.3389/FIMMU.2015.00030/ABSTRACT.
89. Pillai, S., Cariappa, A., 2009. The follicular versus marginal zone B lymphocyte cell fate decision. Nat. Rev. Immunol. 2009 9:11 9, 767–777. https://doi.org/10.1038/nri2656.
90. Demento, S.L., Cui, W., Criscione, J.M., Stern, E., Tulipan, J., Kaech, S.M., Fahmy, T.M., 2012. Role of sustained antigen release from nanoparticle vaccines in shaping the T cell memory phenotype. Biomaterials 33, 4957–4964. https://doi.org/10.1016/J.BIOMATERIALS.2012.03.041.
91. Reed, S.G., Orr, M.T., Fox, C.B., 2013. Key roles of adjuvants in modern vaccines. Nat. Med. 19:12, 1597–1608. https://doi.org/10.1038/nm.3409.
92. Zhao, L., Seth, A., Wibowo, N., Zhao, C.X., Mitter, N., Yu, C., Middelberg, A.P.J., 2014. Nanoparticle vaccines. Vaccine 32, 327–337. https://doi.org/10.1016/J.VACCINE.2013.11.069.
93. Jia, J., Zhang, Y., Xin, Y., Jiang, C., Yan, B., Zhai, S., 2018. Interactions Between Nanoparticles and Dendritic Cells: From the Perspective of Cancer Immunotherapy. Front. Oncol. 8, 410678. https://doi.org/10.3389/FONC.2018.00404/BIBTEX.
94. Liu, J., Miao, L., Sui, J., Hao, Y., Huang, G., 2020. Nanoparticle cancer vaccines: Design considerations and recent advances. Asian J. Pharm. Sci. 15, 576–590. https://doi.org/10.1016/J.AJPS.2019.10.006.
95. Wang, Yongchao, Wang, J., Zhu, D., Wang, Yufei, Qing, G., Zhang, Y., Liu, X., Liang, X.J., 2021. Effect of physicochemical properties on in vivo fate of nanoparticle-based cancer immunotherapies. Acta Pharm. Sin. B 11, 886–902. https://doi.org/10.1016/J.APSB.2021.03.007
96. Getts, D.R., Shea, L.D., Miller, S.D., King, N.J.C., 2015. Harnessing nanoparticles for immune modulation. Trends Immunol. 36, 419–427. https://doi.org/10.1016/J.IT.2015.05.007.
97. Moyano, D.F., Liu, Y., Peer, D., Rotello, V.M., 2016. Modulation of Immune Response Using

Engineered Nanoparticle Surfaces. Small 12, 76–82. https://doi.org/10.1002/SMLL.201502273.
98. Correia-Pinto, J.F., Csaba, N., Alonso, M.J., 2013. Vaccine delivery carriers: Insights and future perspectives. Int. J. Pharm. 440, 27–38. https://doi.org/10.1016/J.IJPHARM.2012.04.047.
99. Fan, Y., Moon, J.J., 2015. Nanoparticle Drug Delivery Systems Designed to Improve Cancer Vaccines and Immunotherapy. Vaccines 3, 662-685. https://doi.org/10.3390/VACCINES3030662.
100. Doddapaneni, B.S., Kyryachenko, S., Chagani, S.E., Alany, R.G., Rao, D.A., Indra, A.K., Alani, A.W.G., 2015. A three-drug nanoscale drug delivery system designed for preferential lymphatic uptake for the treatment of metastatic melanoma. J. Control. Release 220, 503–514. https://doi.org/10.1016/J.JCONREL.2015.11.013.
101. Min, Y., Roche, K.C., Tian, S., Eblan, M.J., McKinnon, K.P., Caster, J.M., Chai, S., Herring, L.E., Zhang, L., Zhang, T., Desimone, J.M., Tepper, J.E., Vincent, B.G., Serody, J.S., Wang, A.Z., 2017. Antigen-capturing nanoparticles improve the abscopal effect and cancer immunotherapy. Nat. Nanotechnol. 2017 12:9 12, 877–882. https://doi.org/10.1038/nnano.2017.113.
102. Foged, C., Brodin, B., Frokjaer, S., Sundblad, A., 2005. Particle size and surface charge affect particle uptake by human dendritic cells in an in vitro model. Int. J. Pharm. 298, 315–322. https://doi.org/10.1016/J.IJPHARM.2005.03.035.
103. Henriksen-Lacey, M., Christensen, D., Bramwell, V.W., Lindenstrøm, T., Agger, E.M., Andersen, P., Perrie, Y., 2010b. Liposomal cationic charge and antigen adsorption are important properties for the efficient deposition of antigen at the injection site and ability of the vaccine to induce a CMI response. J. Control. Release 145, 102–108. https://doi.org/10.1016/J.JCONREL.2010.03.027.
104. Christensen, D., Henriksen-Lacey, M., Kamath, A.T., Lindenstrøm, T., Korsholm, K.S., Christensen, J.P., Rochat, A.F., Lambert, P.H., Andersen, P., Siegrist, C.A., Perrie, Y., Agger, E.M., 2012. A cationic vaccine adjuvant based on a saturated quaternary ammonium lipid have different in vivo distribution kinetics and display a distinct CD4 T cell-inducing capacity compared to its unsaturated analog. J. Control. Release 160, 468–476. https://doi.org/10.1016/j.jconrel.2012.03.016.
105. Merkel, T.J., Jones, S.W., Herlihy, K.P., Kersey, F.R., Shields, A.R., Napier, M., Luft, J.C., Wu, H., Zamboni, W.C., Wang, A.Z., Bear, J.E., DeSimone, J.M., 2011. Using mechanobiological mimicry of red blood cells to extend circulation times of hydrogel microparticles. Proc. Nat. Acad. Sci. 108, 586–591. https://doi.org/10.1073/PNAS.1010013108.
106. Anselmo, A.C., Zhang, M., Kumar, S., Vogus, D.R., Menegatti, S., Helgeson, M.E., Mitragotri, S., 2015. Elasticity of nanoparticles influences their blood circulation, phagocytosis, endocytosis, and targeting. ACS Nano 9, 3169–3177. https://doi.org/10.1021/acsnano.5b00147.
107. Sun, J., Zhang, L., Wang, J., Feng, Q., Liu, D., Yin, Q., Xu, D., Wei, Y., Ding, B., Shi, X., Jiang, X., 2015. Tunable Rigidity of (Polymeric Core)–(Lipid Shell) Nanoparticles for Regulated Cellular Uptake. Adv. Mater. 27, 1402–1407. https://doi.org/10.1002/ADMA.201404788.
108. Moyano, D.F., Goldsmith, M., Solfiell, D.J., Landesman-Milo, D., Miranda, O.R., Peer, D., Rotello, V.M., 2012. Nanoparticle hydrophobicity dictates immune response. J. Am. Chem. Soc. 134, 3965–3967. https://doi.org/10.1021/JA2108905.
109. Rao, D.A., Forrest, M.L., Alani, A.W.G., Kwon, G.S., Robinson, J.R., 2010. Biodegradable PLGA based nanoparticles for sustained regional lymphatic drug delivery. J. Pharm. Sci. 99, 2018–2031. https://doi.org/10.1002/JPS.21970.
110. Flynn, J.A.L., 2004. Immunology of tuberculosis and implications in vaccine development. Tuberculosis 84, 93–101. https://doi.org/10.1016/J.TUBE.2003.08.010.
111. Griffiths, K.L., Khader, S.A., 2014. Novel vaccine approaches for protection against intracellular pathogens. Curr. Opin. Immunol. 28, 58–63. https://doi.org/10.1016/J.COI.2014.02.003.
112. Ottenhoff, T.H.M., Lewinsohn, D.A., Lewinsohn, D.M., 2008. Human CD4 and CD8 T Cell Responses to Mycobacterium tuberculosis: Antigen Specificity, Function, Implications and Applications, in: Handbook of Tuberculosis, 119–155. https://doi.org/10.1002/9783527611614.CH23.
113. Henao-Tamayo, M.I., Ordway, D.J., Irwin, S.M., Shang, S., Shanley, C., Orme, I.M., 2010. Phenotypic definition of effector and memory T-lymphocyte subsets in mice chronically infected with mycobacterium tuberculosis. Clin. Vaccine Immunol. 17, 618–625. https://doi.org/10.1128/CVI.00368-09.
114. Kipnis, A., Irwin, S., Izzo, A.A., Basaraba, R.J., Orme, I.M., 2005. Memory T Lymphocytes Generated by Mycobacterium bovis BCG Vaccination Reside within a CD4 CD44lo CD62 Ligandhi Population. Infect. Immun. 73, 7759. https://doi.org/10.1128/IAI.73.11.7759-7764.2005.
115. Orme, I.M., 2010. The Achilles heel of BCG. Tuberculosis 90, 329–332. https://doi.org/10.1016/J.TUBE.2010.06.002.
116. Lu, Y.J., Barreira-Silva, P., Boyce, S., Powers, J., Cavallo, K., Behar, S.M., 2021. CD4 T cell help prevents CD8 T cell exhaustion and promotes control of Mycobacterium tuberculosis infection. Cell Rep. 36, 109696. https://doi.org/10.1016/J.CELREP.2021.109696.
117. Prezzemolo, T., Guggino, G., La Manna, M.P., Di Liberto, D. Di, Dieli, F., Caccamo, N., 2014. Functional signatures of human CD4 and CD8 T cell responses to Mycobacterium tuberculosis. Front. Immunol. 5, 83298. https://doi.org/10.3389/FIMMU.2014.00180/BIBTEX.
118. Behar, S.M., Woodworth, J.S.M., Wu, Y., 2007. Next generation: tuberculosis vaccines that elicit protective CD8+ T cells. Expert Rev. Vaccines 6, 441–456. https://doi.org/10.1586/14760584.6.3.441.
119. Boom, W.H., 2007. New TB vaccines: is there a requirement for CD8+ T cells? J. Clin. Invest. 117, 2092–2094. https://doi.org/10.1172/JCI32933.
120. Behar, S.M., Dascher, C.C., Grusby, M.J., Wang, C.R., Brenner, M.B., 1999. Susceptibility of Mice Deficient in CD1D or TAP1 to Infection with Mycobacterium tuberculosis. J. Exp. Med. 189, 1973–1980. https://doi.org/10.1084/JEM.189.12.1973.
121. Flynn, J.L., Goldstein, M.M., Triebold, K.J., Koller, B., Bloom, B.R., 1992. Major histocompatibility complex class I-restricted T cells are required for resistance to Mycobacterium tuberculosis infection. Proc. Nat. Acad. Sci. 89, 12013–12017. https://doi.org/10.1073/PNAS.89.24.12013.
122. Orme, I.M., 1987. The kinetics of emergence and loss of mediator T lymphocytes acquired in response to infection with Mycobacterium tuberculosis. J. Immunol. 138, 293–298. https://doi.org/10.4049/JIMMUNOL.138.1.293.
123. Sousa, A.O., Mazzaccaro, R.J., Russell, R.G., Lee, F.K., Turner, O.C., Hong, S., Van Kaer, L., Bloom, B.R., 2000. Relative contributions of distinct MHC class I-dependent cell populations in protection to tuberculosis infection in mice. Proc. Nat. Acad. Sci. 97, 4204–4208. https://doi.org/10.1073/PNAS.97.8.4204.
124. Van Pinxteren, L.A.H., Cassidy, J.P., Smedegaard, B.H.C., Agger, E.M., Andersen, P., 2000. Control of latent Mycobacterium tuberculosis infection is dependent on CD8 T cells. Eur. J. Immunol. 30, 3689–3698. https://doi.org/10.1002/1521-4141.
125. Lin, P.L., Rutledge, T., Green, A.M., Bigbee, M., Fuhrman, C., Klein, E., Flynn, J.L., 2012. CD4 T Cell Depletion Exacerbates Acute Mycobacterium tuberculosis While Reactivation of Latent Infection Is Dependent on Severity of Tissue Depletion in Cynomolgus Macaques. AIDS Res. Hum. Retroviruses 28, 1693–1702. https://doi.org/10.1089/AID.2012.0028.
126. Ciric, B., El-behi, M., Cabrera, R., Zhang, G.-X., Rostami, A., 2009. IL-23 Drives Pathogenic IL-17-Producing CD8+ T Cells. J. Immunol. 182, 5296–5305. https://doi.org/10.4049/JIMMUNOL.0900036.
127. Mills, K.H.G., 2022. IL-17 and IL-17-producing cells in protection versus pathology. Nat. Rev. Immunol. 2022 23:1 23, 38–54. https://doi.org/10.1038/s41577-022-00746-9.
128. Ernst, J.D., 2012. The immunological life cycle of tuberculosis. Nat. Rev. Immunol. 2012 12:8 12, 581–591. https://doi.org/10.1038/nri3259.
129. Duong, V.T., Skwarczynski, M., Toth, I., 2023b. Towards the development of subunit vaccines against tuberculosis: The key role of adjuvant. Tuberculosis 139, 102307. https://doi.org/10.1016/J.TUBE.2023.102307.
130. Rijnink, W.F., Ottenhoff, T.H.M., Joosten, S.A., 2021. B-Cells and Antibodies as Contributors to Effector Immune Responses in Tuberculosis. Front. Immunol. 12, 640168. https://doi.org/10.3389/FIMMU.2021.640168/BIBTEX
131. Maglione, P.J., Xu, J., Chan, J., 2007. B Cells Moderate Inflammatory Progression and Enhance Bacterial Containment upon Pulmonary Challenge with Mycobacterium tuberculosis. J. Immunol. 178, 7222–7234. https://doi.org/10.4049/JIMMUNOL.178.11.7222.
132. Phuah, J., Wong, E.A., Gideon, H.P., Maiello, P., Coleman, M.T., Hendricks, M.R., Ruden, R., Cirrincione, L.R., Chan, J., Lin, P.L., Flynn, J.A.L., 2016. Effects of B cell depletion on early Mycobacterium tuberculosis infection in cynomolgus macaques. Infect. Immun. 84, 1301–1311. https://doi.org/10.1128/iai.00083-16.
133. Vordermeier, H.M., Venkataprasad, N., Harris, D.P., Ivanyi, J., 2003. Increase of tuberculous infection in the organs of B cell-deficient mice. Clin. Exp. Immunol. 106, 312–316. https://doi.org/10.1046/J.1365-2249.1996.D01-845.X.

134. Joosten, S.A., van Meijgaarden, K.E., del Nonno, F., Baiocchini, A., Petrone, L., Vanini, V., Smits, H.H., Palmieri, F., Goletti, D., Ottenhoff, T.H.M., 2016. Patients with Tuberculosis Have a Dysfunctional Circulating B-Cell Compartment, Which Normalizes following Successful Treatment. PLoS Pathog. 12, e1005687. https://doi.org/10.1371/JOURNAL.PPAT.1005687.
135. Bosio, C.M., Gardner, D., Elkins, K.L., 2000. Infection of B Cell-Deficient Mice with CDC 1551, a Clinical Isolate of Mycobacterium tuberculosis: Delay in Dissemination and Development of Lung Pathology. J. Immunol. 164, 6417–6425. https://doi.org/10.4049/JIMMUNOL.164.12.6417.
136. Johnson, C.M., Cooper, A.M., Frank, A.A., Bonorino, C.B.C., Wysoki, L.J., Orme, I.M., 1997. Mycobacterium tuberculosis aerogenic rechallenge infections in B cell-deficient mice. Tuberc. Lung Dis. 78, 257–261. https://doi.org/10.1016/S0962-8479(97)90006-X.
137. Turner, J., Frank, A.A., Brooks, J. V., Gonzalez-Juarrero, M., Orme, I.M., 2001. The progression of chronic tuberculosis in the mouse does not require the participation of B lymphocytes or interleukin-4. Exp. Gerontol. 36, 537–545. https://doi.org/10.1016/S0531-5565(00)00257-6.
138. Li, H., Wang, X.X., Wang, B., Fu, L., Liu, G., Lu, Y., Cao, M., Huang, H., Javid, B., 2017. Latently and uninfected healthcare workers exposed to TB make protective antibodies against Mycobacterium tuberculosis. Proc. Nat. Acad. Sci. 114, 5023–5028. https://doi.org/10.1073/pnas.1611776114.
139. Balu, S., Reljic, R., Lewis, M.J., Pleass, R.J., McIntosh, R., van Kooten, C., van Egmond, M., Challacombe, S., Woof, J.M., Ivanyi, J., 2011. A Novel Human IgA Monoclonal Antibody Protects against Tuberculosis. J. Immunol. 186, 3113–3119. https://doi.org/10.4049/JIMMUNOL.1003189.
140. Hamasur, B., Haile, M., Pawlowski, A., Schröder, U., Källenius, G., Svenson, S.B., 2004. A mycobacterial lipoarabinomannan specific monoclonal antibody and its F(ab´)2 fragment prolong survival of mice infected with Mycobacterium tuberculosis. Clin. Exp. Immunol. 138, 30–38. https://doi.org/10.1111/J.1365-2249.2004.02593.X.
141. López, Y., Yero, D., Falero-Diaz, G., Olivares, N., Sarmiento, M.E., Sifontes, S., Solis, R.L., Barrios, J.A., Aguilar, D., Hernández-Pando, R., Acosta, A., 2009. Induction of a protective response with an IgA monoclonal antibody against Mycobacterium tuberculosis 16 kDa protein in a model of progressive pulmonary infection. Int. J. Med. Microbiol. 299, 447–452. https://doi.org/10.1016/J.IJMM.2008.10.007.
142. Zimmermann, N., Thormann, V., Hu, B., Köhler, A., Imai-Matsushima, A., Locht, C., Arnett, E., Schlesinger, L.S., Zoller, T., Schürmann, M., Kaufmann, S.H., Wardemann, H., 2016. Human isotype-dependent inhibitory antibody responses against Mycobacterium tuberculosis. EMBO Mol. Med. 8, 1325–1339. https://doi.org/10.15252/EMMM.201606330.
143. Lu, L.L., Chung, A.W., Rosebrock, T.R., Ghebremichael, M., Yu, W.H., Grace, P.S., Schoen, M.K., Tafesse, F., Martin, C., Leung, V., Mahan, A.E., Sips, M., Kumar, M.P., Tedesco, J., Robinson, H., Tkachenko, E., Draghi, M., Freedberg, K.J., Streeck, H., Suscovich, T.J., Lauffenburger, D.A., Restrepo, B.I., Day, C., Fortune, S.M., Alter, G., 2016. A Functional Role for Antibodies in Tuberculosis. Cell 167, 433-443.e14. https://doi.org/10.1016/J.CELL.2016.08.072.
144. Kagina, B.M.N., Abel, B., Scriba, T.J., Hughes, E.J., Keyser, A., Soares, A., Gamieldien, H., Sidibana, M., Hatherill, M., Gelderbloem, S., Mahomed, H., Hawkridge, A., Hussey, G., Kaplan, G., Hanekom, W.A., 2012. Specific T Cell Frequency and Cytokine Expression Profile Do Not Correlate with Protection against Tuberculosis after Bacillus Calmette-Guérin Vaccination of Newborns. Am. J. Respir. Crit. Care Med. 182, 1073–1079. https://doi.org/10.1164/RCCM.201003-0334OC.
145. Mittrücker, H.W., Steinhoff, U., Köhler, A., Krause, M., Lazar, D., Mex, P., Miekley, D., Kaufmann, S.H.E., 2007. Poor correlation between BCG vaccination-induced T cell responses and protection against tuberculosis. Proc. Nat. Acad. Sci. 104, 12434–12439. https://doi.org/10.1073/pnas.0703510104.



# SUPPLEMENTARY MATERIAL

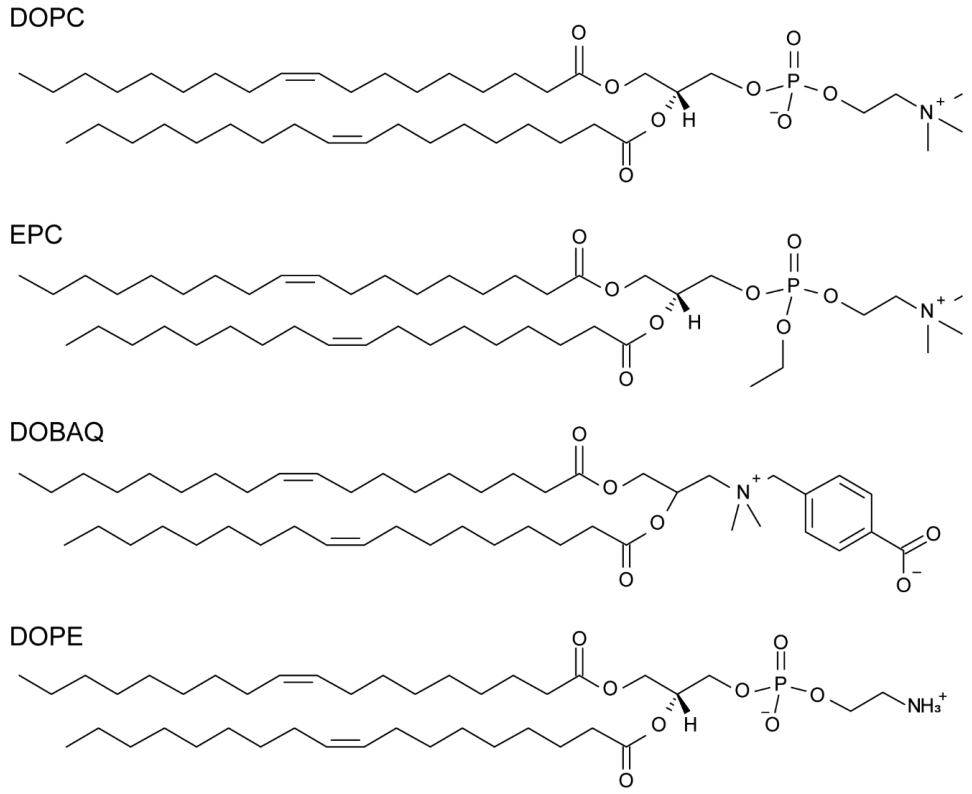


**Figure S1**. Chemical structures of lipids used in production of pH-sensitive liposomes and lipid-PLGA hybrid NPs.

**Table S1**. List of antibodies used for spectral flow cytometry analysis of $CD4^+$, $CD8^+$, and $CD3^-$ $CD19^+$ cells.

| Marker | Fluorochrome | Clone | Catalog | Manufacturer |
|---|---|---|---|---|
| CCR7 (CD197) | PE/Cyanine5 | 4B12 | 120113 | BioLegend |
| CD273 | Brilliant Ultra Violet (BUV) 395 | TY25 | 565102 | BD Biosciences |
| CD8b.2 | BUV 496 | 53-5.8 | 741049 | BD Biosciences |
| CD80 | BUV 661 | 16-10A1 | 741515 | BD Biosciences |
| CD69 | BUV 737 | H1.2F3 | 612793 | BD Biosciences |
| CD25 | Brilliant Violet (BV) 480 | PC61 | 566120 | BD Biosciences |
| CD154 | Super Bright 436 | MR1 | 62-1541-82 | Thermo Fisher |
| IgD | Pacific Blue | 11-26c.2a | 405711 | BioLegend |
| I-A/I-E (MHC II) | BV 510 | M5/114.15.2 | 107636 | BioLegend |
| CD44 | BV 570 | IM7 | 103037 | BioLegend |
| PD-1 (CD279) | BV 605 | 29F.1A12 | 135220 | BioLegend |
| CXCR3 (CD183) | BV 650 | CXCR3-173 | 126531 | BioLegend |
| KLRG1 (MAFA) | BV 711 | 2F1/KLRG1 | 138427 | BioLegend |
| CCR6 (CD196) | BV 785 | 29-2L17 | 129823 | BioLegend |
| CD4 | Spark Blue 550 | GK1.5 | 100474 | BioLegend |
| CCR5 (CD195) | PerCP/Cyanine5.5 | HM-CCR5 | 107015 | BioLegend |
| CD19 | PE Fire 640 | 6D5 | 115574 | BioLegend |
| CD138 | APC | 281-2 | 142505 | BioLegend |
| B220 (CD45R) | Spark NIR 685 | RA3-6B2 | 103267 | BioLegend |
| CD62L (L-selectin) | APC/Fire 750 | MEL-14 | 104449 | BioLegend |
| CD3 | APC/Fire 810 | 17A2 | 100267 | BioLegend |
| IL-2 | APC-R700 | JES6-5H4 | 565186 | BD Biosciences |
| IL-17A | PE | eBio17B7 | 12-7177-81 | Thermo Fisher |
| IgM | FITC | RMM-1 | 406505 | BioLegend |
| IL-10 | PE/Dazzle 594 | JES5-16E3 | 505033 | BioLegend |
| TNFα | PE/Cyanine7 | MP6-XT22 | 506323 | BioLegend |
| IFNγ | Alexa Fluor 647 | XMG1.2 | 505816 | BioLegend |

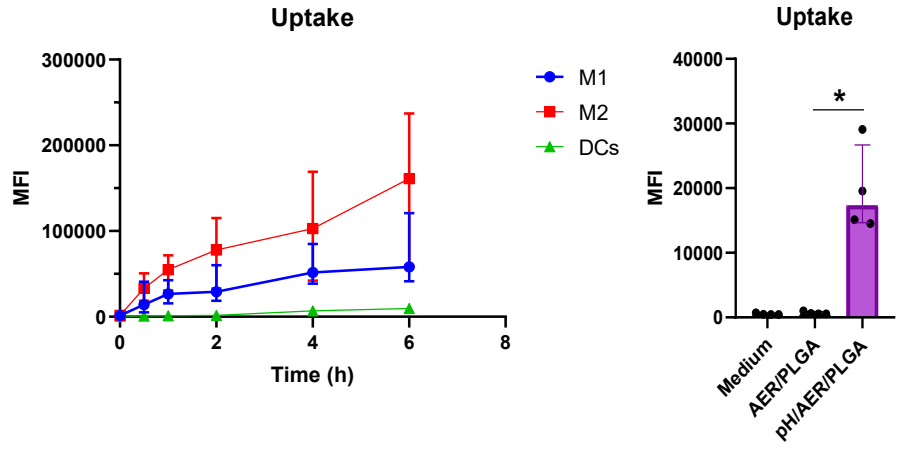


**Figure S2**. Uptake of (DiI-stained) PLGA NPs and lipid-PLGA hybrid NPs. A) Uptake kinetics of PLGA NPs by MDDCs, pro-inflammatory (M1), and anti-inflammatory M2 MDMFs between 1 and 6 hours of exposure. n = 4 (MDMFs), n =2 (MDDCs) donors. B) Uptake of PLGA NPs and lipid-PLGA hybrid NPs by MDDCs after 1 h of exposure. n = 4 donors. Results represent median fluorescence intensity (MFI) ± IQR.

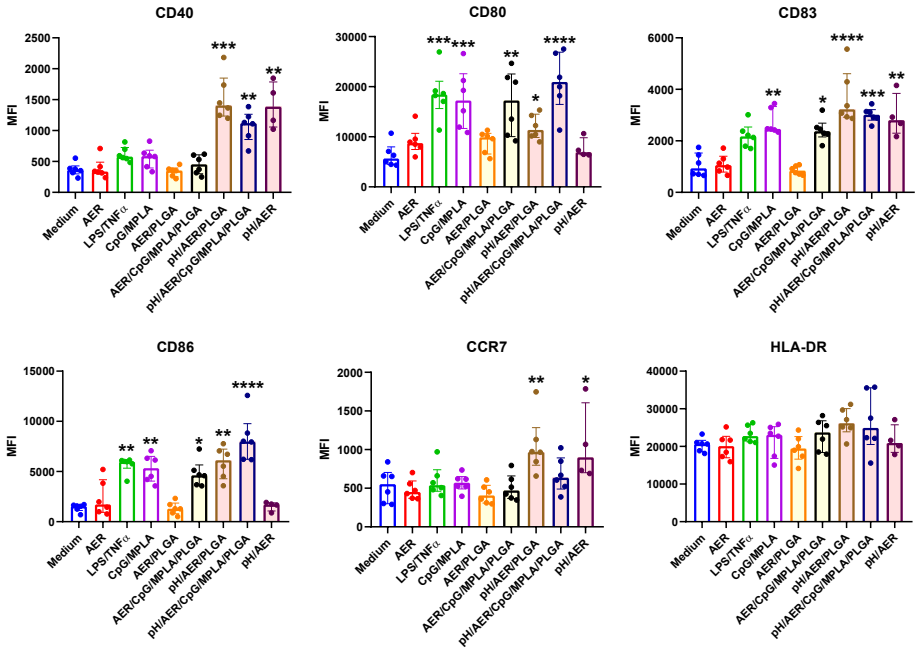


**Figure S3**. Cell surface activation marker expression levels in MDDCs after stimulation with medium, unadjuvanted AER (5 μg/ml), a combination of LPS and TNFα (100 and 5 ng/ml, respectively), CpG and MPLA (1.56 and 0.625 μg/ml, respectively) as the positive controls, and vaccine formulations: PLGA NPs (5 μg/ml AER, 250 μg/ml PLGA), lipid-PLGA hybrid NPs (5 μg/ml AER, 250 μg/ml lipids, 250 μg/ml PLGA), and (pH) liposomal formulation (5 μg/ml AER, 250 μg/ml liposomes), and their adjuvanted counterparts (containing additionally 1.56 and 0.625 μg/ml CpG and MPLA, respectively). Median fluorescence intensities (MFI) related to the expression of indicated activation markers. The formulations are compared to the medium in the significance testing. The results represent median ± IQR. n = 4 or 6 (cell donors).



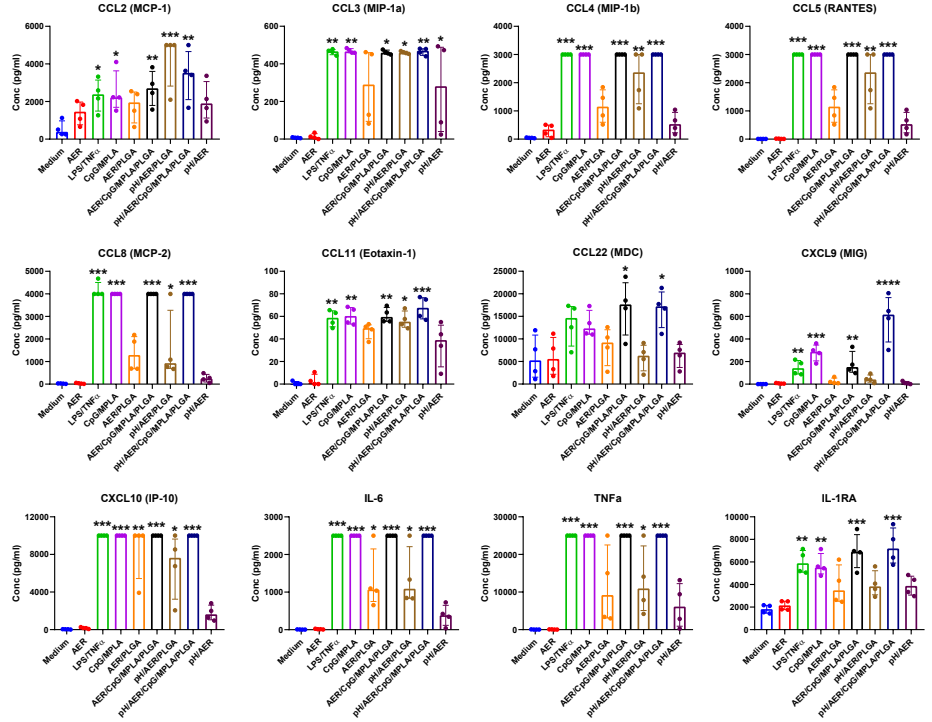


**Figure S4**. Production of cytokines by MDDCs exposed to vaccine formulations. Concentrations used: 5 μg/ml AER, 100 ng/ml LPS and 5 ng/ml TNFα, 1.56 μg/ml CpG and 0.625 μg/ml MPLA, 250 μg/ml PLGA, 250 μg/ml liposomes/lipids, exposure 1 hour, n = 4 (cell donors). The results represent median ± IQR.

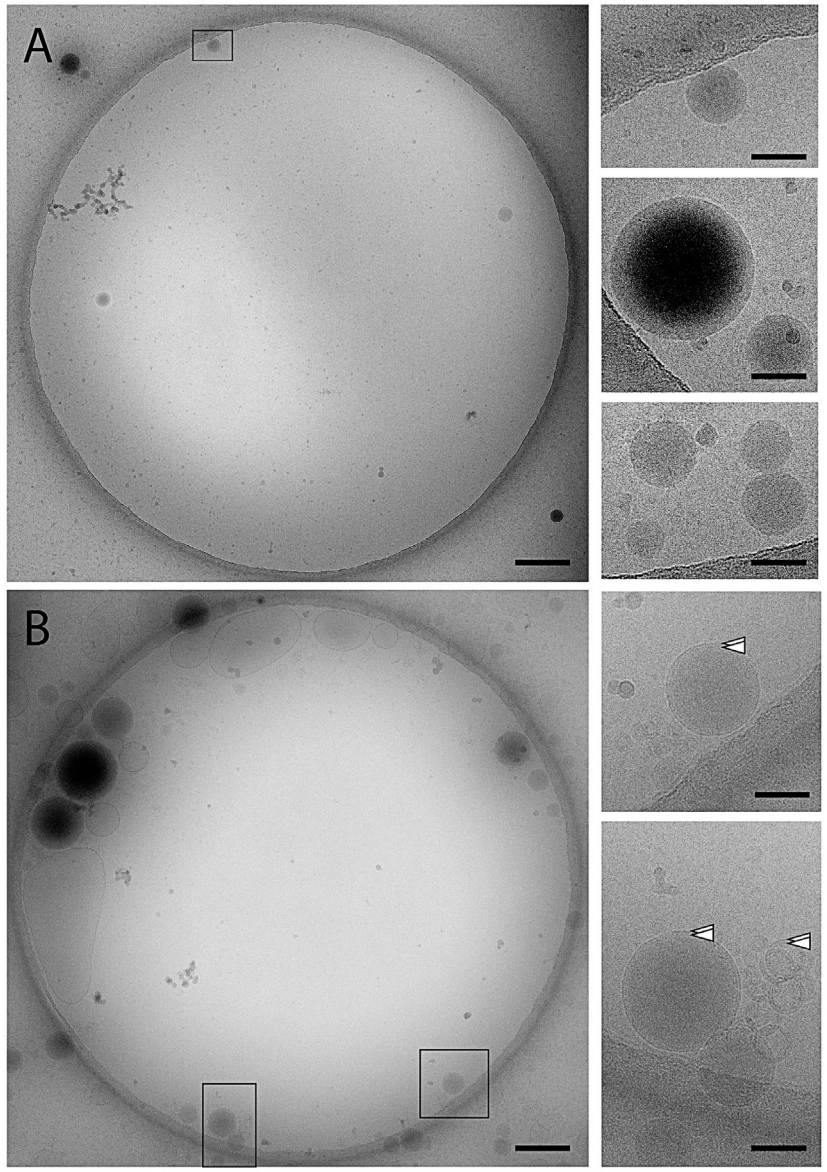


**Figure S5**. A) PLGA NPs (without lipids added). CryoEM overview image of a typical 2-micron diameter hole in the carbon film with three PLGA spheres. The box's area is magnified on the top right. Several other spheres from other images are shown below that image. The edges of the spheres are not sharply defined. B) Lipid-PLGA hybrid NPs. CryoEM overview of a typical 2-micron diameter hole in the carbon film showing multiple lipid-PLGA spheres. Irregularly shaped lipid vesicles were found occasionally. The boxes' areas are magnified and show PLGA spheres with clear lipid bilayer-resembling features, which can also be observed in small lipid vesicles (arrowheads). The borders of the spheres are more distinctive. In both A and B scale bars are 200 nm (overview images) and 50 nm (insets).



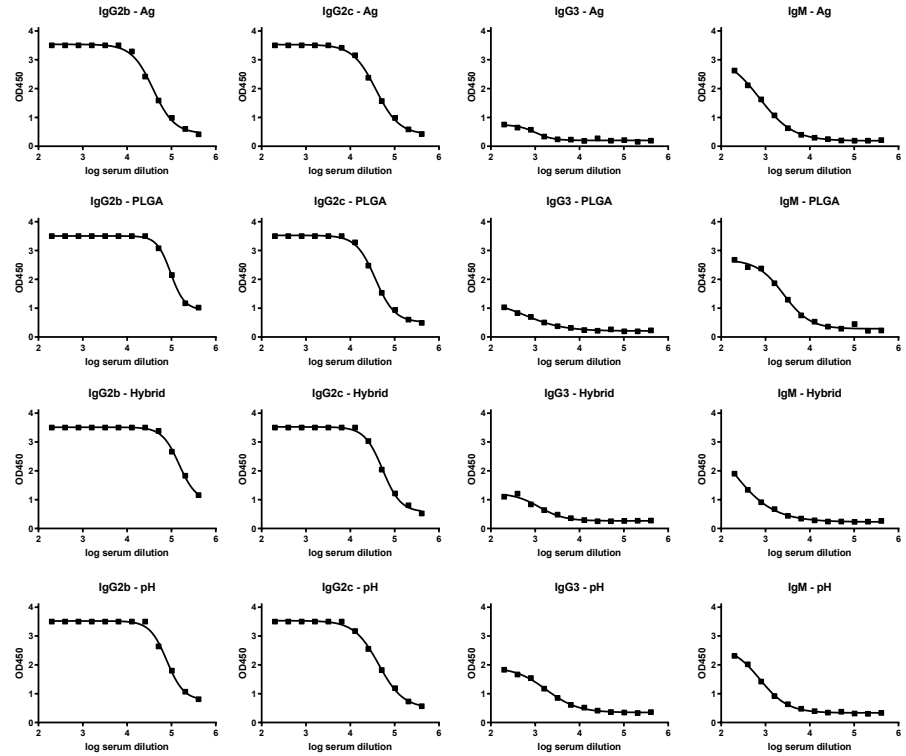


**Figure S6**. Quantification of AER-specific antibodies in sera. The type of antibody measured is indicated above each graph as well as the vaccination group. Values represent OD450 ELISA, and serum dilutions are shown on the x-axis. Groups are indicated in the legend. Naïve controls were not included because of the undetected (total) AER-specific antibodies (Figure 7). n = 2 (mice).